

# A Scalable Thermal Reservoir Simulator for Giant Models on Parallel Computers

Hui Liu\*, Zhangxin Chen

Dept. of Chemical and Petroleum Engineering, University of Calgary  
2500 University Drive NW, Calgary, AB, Canada

## Abstract

This paper introduces the model, numerical methods, algorithms and parallel implementation of a thermal reservoir simulator that designed for numerical simulations of thermal reservoir with multiple components in three dimensional domain using distributed-memory parallel computers. The full model is introduced with correlations for important properties and well modeling. Various well constraints, such as fixed bottom hole pressure, fix oil, water, gas and liquid rates, constant heat transfer model, convective heat transfer model, heater model (temperature control, rate control, dual rate/temperature control, and subcool (steam trap)), are introduced in detail, including their mathematical models and methods. Efficient numerical methods and parallel computing technologies are presented. Numerical experiments show that our results match commercial simulators, which confirms the correctness of our methods and implementations. Scalability testings demonstrate that our simulator can handle giant thermal models with billions of grid blocks and the simulator has excellent scalability.

## 1 Introduction

Reservoir simulations play critical roles in reservoir management, since it provides one way to examine production plan and to predict future oil and gas production. Simulators have been developed and applied for decades, such as CMG STARS. They have widely used in reservoir management. When multiple chemicals are considered in a model or the geological model is complicated, it may take too long for one simulation, which reduces the productivity of reservoir engineers. Acceleration of simulations is important to oil and gas industry.

Reservoir simulations have been studied for decades, and various models and methods have been proposed. Crookston et al.[11] proposed a simple two-dimensional model to deal with three phases flow and to handle vaporization-condensation effects. Grabowski [18] developed a sequential implicit method for thermal reservoir model. A general four-phase multi-component in-situ combustion model was proposed by Coats [8], which was improved by Rubin [27] that a fully coupled implicit wellbore model was considered. Variable substitution [8] methods and pseudo-equilibrium ratio (PER) methods [11] were designed to discretize the thermal models, while Miffin et al[25] suggested to use global variables, pressure, moles and energy as unknowns. Barua [5] proposed algorithms to solve the nonlinear equations in parallel and combined the iterative solutions to linear systems and Quasi-Newton method. Effective linear solver and preconditioner methods have been proposed to accelerate the solution of linear systems from reservoir simulations, such as constrained pressure residual (CPR) methods [29, 6], multi-stage methods [3], multiple level preconditioners [30] and FASP (fast auxiliary space preconditioners) [19, 16]. Chen et al. designed a family of CPR-like preconditioners, such as CPR-FP, CPR-FPF and CPR-FFPF methods [21], which have been applied to different simulations [33, 23, 22, 34].

Parallel computers have more memory and higher performance, which provide excellent approaches to accelerate reservoir simulations [12, 10, 37, 15]. In the early stage, vectorization techniques in shared-memory machines was widely applied though it didn't scale very well [9, 12]. Meijerink [24] developed a black oil simulator using the IMPES method and implemented on a local-memory MIMD computer. Chien [7] applied domain decomposition and MPI on an IBM SP-2 parallel computer. Wang [36, 26] implemented a fully implicit equation-of-state compositional simulator for distributed-memory parallel computers, and large-scale reservoir models were simulated [35]. Reservoir models with millions of grid blocks on parallel computers

---

\*Authors to whom correspondence may be addressed. Email: hui.sc.liu@gmail.com

were reported[28]. Killough [20] reviewed the parallel reservoir models and parallel computing technologies. Saudi Aramco developed new-generation massively-parallel reservoir simulator [4, 13, 14, 17], and reservoir models with millions of grid blocks were studied. Zhang et al. developed a scalable general-purpose platform, which has been applied to reservoir simulations [38, 39, 31].

The structure of the paper is as follows. In §2, the thermal reservoir model is introduced and the equations for various properties are presented. In §3, numerical methods and parallel computing approaches are proposed. In §4, numerical experiments are carried out to validate our results against commercial simulator, CMG STARS, and to show the scalability of the parallel thermal simulator.

## 2 Mathematical Model

For the sake of completeness, the mathematical model of the thermal simulator is introduced here, and the content of this section is borrowed from our previous manuscript [1]. In reference [1], the following assumptions were made: water component exists in water and gas phases, all oil components exist in oil and gas phases, non-condensable gas components exist in gas phase only, and all three phases co-exist during the entire simulation. In this paper, different assumptions are made: the water component exists in water and gas phases, heavy oil components exist in oil phase only, light oil components exist in both oil and gas phases, non-condensable gas components exist in gas phase. Phase appearance and dis-appearance are allowed. Depending on the input, arbitrary oil components and non-condensable gas components are allowed. Necessary changes have been made to address the difference between the in-situ combustion model [1] and the thermal model applied here.

### 2.1 Darcys Law

Darcy's law is applied to model the velocity of a fluid phase, which describes the relation among permeability, viscosity, saturation and pressure difference. In our thermal model, the water phase ( $w$ ), the oil phase ( $o$ ) and the gas phase ( $g$ ) co-exist, ([40]),

$$\begin{aligned}\vec{u}_w &= -\frac{k_{rw}}{\mu_w} \vec{k} (\nabla p_w - \gamma_w \nabla z) \\ \vec{u}_o &= -\frac{k_{ro}}{\mu_o} \vec{k} (\nabla p_o - \gamma_o \nabla z) \\ \vec{u}_g &= -\frac{k_{rg}}{\mu_g} \vec{k} (\nabla p_g - \gamma_g \nabla z).\end{aligned}\tag{1}$$

### 2.2 Mass Conservation Equations

For a multi-phase, multi-component system,  $x_{c,\alpha}$  denotes the mole fraction of a component in the  $\alpha$ -phase. The molar number of a component in a phase and the total molar number of the phase are denoted as  $n_{c,\alpha}$  and  $n_\alpha$ , respectively. Thus the molar fractions are

$$x_{c,\alpha} = \frac{n_{c,\alpha}}{n_\alpha}.\tag{2}$$

In the simplest thermal model, water phase has water component only, so  $n_w = 1$ . If the gas phase exists, it may contains water, light oil and non-condensable gas components. Since each component may exist in several phases, total molar number of component  $c$  is written as below ([40]):

$$\frac{\partial}{\partial t} (\phi \Sigma_\alpha^{N_\alpha} \rho_\alpha S_\alpha x_{c,\alpha}) = -\nabla \cdot (\Sigma_\alpha^{N_\alpha} \rho_\alpha S_\alpha \vec{u}_\alpha) + \Sigma_\alpha^{N_\alpha} q_{\alpha,well} x_{c,\alpha}.\tag{3}$$

In this equation, it is noticeable that different from other models, the mass conserved here is only the molar number rather than the mass. Also,  $\rho_\alpha$  and  $q_\alpha$  are the molar density and molar production/injection of phase  $\alpha$ .

## 2.3 Energy Conservation Equation

The energy conservation equation for a thermal process ([40]) is described as:

$$\begin{aligned} & \frac{\partial}{\partial t} (\phi(\rho_w S_w U_w + \rho_o S_o U_o + \rho_g S_g U_g) + (1 - \phi)U_r) \\ = & \nabla \cdot (K_T \nabla T) - \nabla \cdot (\rho_w H_w \vec{u}_w + \rho_o H_o \vec{u}_o + \rho_g H_g \vec{u}_g) \\ & + (q_{w,well} H_w + q_{o,well} H_o + q_{g,well} H_g) - Q_{loss}, \end{aligned} \quad (4)$$

where  $U$  denotes the volumetric internal energy. On the right-hand side, the first term represents the conduction term. This is caused by a difference in temperature, where the rate of conduction is constraint by  $K_T$ , the bulk thermal conductivity. The thermal conductivity here is a combination of liquid, and rock, where a linear mixing rule is applied ([41]),

$$K_T = \phi [S_w K_w + S_o K_o + S_g K_g] + (1 - \phi) K_r. \quad (5)$$

In the equation,  $K_w, K_o, K_g, K_r$  denote thermal conductivities for water phase, oil phase, gas phase, and rock separately. This rule is also called simple mixing rule in CMG STARS. The complex mixing rule is also implemented in the simulator, whose details can be read from CMG STARS manual. We should mention that there are different ways to model rock internal energy:  $(1 - \phi)U_r$ . In above equation, the porosity,  $\phi$ , is a function of pressure and temperature, and  $U_r$  is a function of temperature, so the rock internal energy is a function of pressure and temperature. This method assumes the volume of a grid block does not change. Another way is to assume the rock volume does not change, which uses  $(1 - \phi_i)U_r$  to model rock internal energy.  $\phi_i$  does not change during the simulation, and this method preserves the rock energy. The second method is applied as the default method in CMG STARS and our simulator.

A heat loss term to underburden and overburden is also considered, and the semi-analytical method developed by Vinsome et al. [59] is applied.

## 2.4 Capillary Pressure

A capillary pressure  $P_c$  is the pressure difference across the interface between two immiscible fluids arising from capillary forces, which are usually functions of saturation, relationship ([40]):

$$p_w = p_o - p_{cow}(S_w), \quad p_g = p_o + p_{cog}(S_g). \quad (6)$$

## 2.5 Phase Composition Constraints

A constraint implies that the sum of all the components' mole fractions in a phase adds up to one, which is usually encountered for in compositional flow ([40]):

$$\sum_{\alpha}^{N_{\alpha}} x_{c,\alpha} = 1, \quad \alpha = w, o, g. \quad (7)$$

It comes from the total mole number of a given phase that

$$\sum_{\alpha}^{N_{\alpha}} n_{c,\alpha} = n_{\alpha}, \quad \alpha = w, o, g. \quad (8)$$

## 2.6 Phase Equilibrium Constraints

In a multi-component system, a K value (or an equilibrium ratio) is defined as the ratio of the mole fractions of a component in its distributed two phases:

$$K_{c,\alpha_1,\alpha_2} = \frac{x_{c,\alpha_1}}{x_{c,\alpha_2}}. \quad (9)$$

In our model, a K value is a function of pressure and temperature, which is calculated from an analytic equation as:

$$K = \left( \frac{kv_1}{p} + kv_2 p + kv_3 \right) \exp \left( \frac{kv_4}{T - kv_5} \right). \quad (10)$$

When gas phase exists, calculations of K-values for water, light oil and heavy oil are as follows ([40]; [41]):

$$\begin{aligned}
K_W &= K_W(p, T) \\
&= \left( \frac{kv1_W}{p} + kv2_W \cdot p + kv3_W \right) \exp \left( \frac{kv4_W}{T - kv5_W} \right), \\
K_{O,i} &= K_O[i](p, T) \\
&= \left( \frac{kv1_{O,i}}{p} + kv2_{O,i} \cdot p + kv3_{O,i} \right) \exp \left( \frac{kv4_{O,i}}{T - kv5_{O,i}} \right). \\
K_{O,i} &= K_O[i](p, T) = 0.
\end{aligned} \tag{11}$$

In our thermal model, the calculations of K-values are modified, where the PER (Pseudo-Equilibrium Ratios) method([52, 51]) is applied for water and light oil,

$$K^*_{*W} = K^*_W(p, T) = \left( \frac{S_w}{S_w + n_{cg}} \right) K_W(p, T), \tag{12}$$

$$K^*_{*O,i} = K^*_O[i](p, T) = \left( \frac{S_o}{S_o + \epsilon} \right) K_O[i](p, T). \tag{13}$$

In calculations of pseudo K-values,  $\epsilon$  is a small number of the order of  $1e - 4$ . The water phase and oil phase exist through the entrie simulation. However, the gas phase is allowed to disappear. The gas phase molar fraction for the oil components and water component are functions of  $p, T, S_w, S_g$ . The molar fraction in the gas phase for gas components are the basic unknowns:

$$y = y(p, T, S_w, S_g). \tag{14}$$

## 2.7 Compressibility Factor of Real Gas

In the thermal model, the Redlich-Kwong EOS ([49]) is used to calculate the Z factor.

$$A = A(p, T) = 0.427480 \left( \frac{p}{p_{crit}} \right) \left( \frac{T_{crit}}{T} \right)^{2.5}, \tag{15}$$

$$B = B(p, T) = 0.086640 \left( \frac{p}{p_{crit}} \right) \left( \frac{T_{crit}}{T} \right). \tag{16}$$

IN addition, the following mixing method is applied:

$$a = \sum_i y_i T_{crit,i} \sqrt{\frac{T_{crit,i}}{p_{crit,i}}}, \tag{17}$$

$$b = \sum_i y_i \frac{T_{crit,i}}{p_{crit,i}}, \tag{18}$$

$$T_{crit} = \left( \frac{a^2}{b} \right)^{\frac{2}{3}}, \tag{19}$$

$$p_{crit} = \frac{T_{crit}}{b}. \tag{20}$$

Then, after we have the coefficients A and B, the compressibility factor of real gas satisfies the equation

$$Z^3 - Z^2 + (A - B - B^2)Z - AB = 0. \tag{21}$$

This equation is cubic. Therefore, there are three roots for the equation. Also, a root might be virtual. In this case, we choose the biggest real root. With the calculation of all the coefficients, the Z factor is a function of  $p, T, x_i$  and  $y_i$ :

$$Z = Z(p, T, x_i, y_i). \tag{22}$$

## 2.8 Density

For real gas mixture, the density of the gas phase can be calculated as:

$$\rho_g = \rho_g(p, T, x_i, y_i) = \frac{p}{Z(p, T, x_i, y_i) \cdot R \cdot T}$$

The water phase only contains one water component in this model, so the calculation of the water density is simple:

$$\rho_w = \rho_w(p, T) = \rho_{w,ref} \exp(cp_w(p - p_{ref}) - ct1_w(T - T_{ref})) \quad (23)$$

$$-\frac{ct2_w}{2}(T - T_{ref})^2 + cpt_w(p - p_{ref})(T - T_{ref})) \quad (24)$$

where  $\rho_{w,ref}$  is the reference density of the water phase at the reference temperature and pressure.

For oil component  $O[i]$  is in the oil phase, the density can be calculated the same:

$$\rho_{O[i]} = \rho_{O[i]}(p, T) = \rho_{O[i],ref} \exp(cp_{O[i]}(p - p_{ref}) - ct1_{O[i]}(T - T_{ref})) \quad (25)$$

$$-\frac{ct2_{O[i]}}{2}(T - T_{ref})^2 + cpt_{O[i]}(p - p_{ref})(T - T_{ref})) \quad (26)$$

The density of oil phase,  $\rho_o$ , which is mixture of multiple oil components, is calculated as:

$$\frac{1}{\rho_o} = \sum_i^{n_{co}} \frac{x_i}{\rho_{O[i]}}. \quad (27)$$

## 2.9 Viscosity

The viscosity of heavy oil is very high, and we assume the viscosity of an oil component is a function of temperature,

$$\mu_{O[i]} = avisc_{O[i]} \exp\left(\frac{bvisc_{O[i]}}{T}\right). \quad (28)$$

The oil phase viscosity is calculated by a logarithmic mixing rule:

$$\ln(\mu_o) = \sum_i^{n_{co}} x[i] \ln(\mu_{O[i]}(T)), \quad (29)$$

which is equivalent to,

$$\mu_o = \mu_o(T, x_i) = \exp\left(\sum_i^{n_{co}} x[i] \ln(\mu_{O[i]}(T))\right) = \sum_i^{n_{co}} (\mu_{O[i]}(T))^{x_i}. \quad (30)$$

The water phase has only one component, and its viscosity is calculated as:

$$\mu_w = \mu_w(T) = avisc_w \exp\left(\frac{bvisc_w}{T}\right). \quad (31)$$

The gas component viscosity is calculated as,

$$\mu_{g,c} = \mu_{g,c}(T) = avg_c \cdot T^{bvg_c}. \quad (32)$$

According to a mixing rule, the molar mass of a component is included:

$$\mu_g = \mu_g(p, T, S_w, S_g, x_i, y_i) = \frac{\sum_c \mu_{g,c} \cdot y_c \sqrt{M_c}}{\sum_c y_c \sqrt{M_c}}. \quad (33)$$

## 2.10 Porosity

Porosity is the ratio of the pore volume to the bulk volume in a porous medium, describing the volume containing fluids. When pressure is high, due to the effort of fluids, pores are also enlarged. For a non-isothermal model, the porosity is also influenced by temperature. We define a coefficient as a total compressibility of porosity ([40]):

$$ctot = ctot(p, T) = cpor(p - p_{ref}) - ctpor(T - T_{ref}) + cptpor(p - p_{ref})(T - T_{ref}). \quad (34)$$

This factor is a function of pressure and temperature. For the calculation of porosity, we have two approaches with this factor:

Linear:

$$\phi = \phi(p, T) = \phi_{ref} \cdot (1 + ctot(p, T)). \quad (35)$$

Nonlinear:

$$\phi = \phi(p, T) = \phi_{ref} \cdot e^{ctot(p, T)}. \quad (36)$$

For both two approaches, porosity is a function of pressure and temperature.

## 2.11 Relative Permeabilities

There are two ways for calculating relative permeabilities. The first one is to use analytical correlations, and the second one is to use input tables. The water phase relative permeability,  $k_{rw}$ , can be obtained with interpolation from oil-water relative permeability table, which is a function of  $S_w$  (and temperature):

$$k_{rw} = k_{rw}(S_w). \quad (37)$$

The gas phase relative permeability,  $k_{rg}$ , can be calculated the same from a gas-oil relative permeability table or gas-liquid relative permeability table, which is a function of  $S_g$  (and temperature):

$$k_{rg} = k_{rg}(S_g). \quad (38)$$

As for the relative permeability of oil  $k_{ro}$ , there are several models available ([46]; [45], 1961; [44]; [43]). In our model, the Stones model II method ([42]) is applied:

$$k_{ro} = k_{ro}(S_w, S_g) \quad (39)$$

$$= k_{rocw} \left[ \left( \frac{k_{row}(S_w)}{k_{rocw}} + k_{rw}(S_w) \right) \left( \frac{k_{rog}(S_g)}{k_{rocw}} + k_{rg}(S_g) \right) - k_{rw}(S_w) - k_{rg}(S_g) \right], \quad (40)$$

where  $k_{rocw}$  is the oil-water two-phase relative permeability to oil at connate water saturation,  $k_{rog}$  is the oil-gas two-phase relative permeability to oil, and  $k_{row}$  is the oil-water two-phase relative permeability to oil.

$$k_{rocw} = k_{row}(S_w = S_{wc}) = k_{rog}(S_g = 0). \quad (41)$$

$k_{row}$  and  $k_{rog}$  are interpolated from input tables.

## 2.12 Energy

Enthalpy is a measurement of energy in a thermodynamic system, which is equal to the internal energy of the system plus the product of pressure and volume. The enthalpy of a gas component is calculated as follows ([41]):

$$H_{g,c} = H_{g,c}(T) = \int_{T_{ref}}^T (cpg1_c + cpg2_c \cdot t + cpg3_c \cdot t^2 + cpg4_c \cdot t^3) dt, \quad (42)$$

$cpgi_c$ ,  $i = 1, 2, 3, 4$ , are constants for component  $c$ . The gas phase enthalpy can be calculated by a weighted mean with gas molar fractions  $y_c$ :

$$H_g = H_g(p, T, S_w, S_g, x_i, y_i) = \sum_c^{N_c} y_c H_{g,c}. \quad (43)$$

For the oil and water phases, the heat of vaporization should be considered, which can be calculated by:

$$H_{v,c} = H_{v,c}(T) = u(T_{crit,c} - T) \cdot hvr_c \cdot (T_{crit,c} - T)^{ev_c}. \quad (44)$$

Here  $u(x)$  denotes the Heaviside unit step function. The enthalpy of a liquid component can be calculated as:

$$H_c = H_c(T) = H_{g,c} - H_{v,c}. \quad (45)$$

where  $H_{g,c}$  is the enthalpy of component  $c$  in the gas phase. As a result, for the water phase which only includes one component, the enthalpy is:

$$H_w = H_w(T) = H_{g,w} - H_{v,w}. \quad (46)$$

For the oil phase, as a mixture, the enthalpy is:

$$H_o = H_o(p, T, x_i) = \sum_i^{n_{co}} x_i (H_{g,O[i]} - H_{v,O[i]}). \quad (47)$$

The internal energy for oil, gas, and water phases ([41]) are calculated as:

$$U_w = U_w(T) = H_w - p/\rho_w, \quad (48)$$

$$U_o = U_o(p, T, x_i) = H_o - p/\rho_o, \quad (49)$$

$$U_g = U_g(p, T, S_w, S_g, x_i, y_i) = H_g - p/\rho_g. \quad (50)$$

For rock, a similar formula is used:

$$U_r = U_r(T) = cp1_r(T - T_{ref}) + \frac{cp2_r}{2}(T^2 - T_{ref}^2). \quad (51)$$

One thing to notice is that the internal energy for rock has a unit of energy per unit volume, while others have energy per unit amount of material. As mentioned above, there are two ways to calculate the volume of rock. The first one assumes the volume of rock (non-null) doesn't change, which is noted as constant rock in CMG STARS. The second one assumes the volume of the grid block doesn't change, which is noted as constant bulk in CMG STARS.

## 2.13 Well Modeling

A Peaceman's model is adopted for well modeling in this paper. A well may have many perforations, and each perforation at a grid cell, its well rate for phase  $\alpha$ ,  $Q_\alpha = Vq_\alpha$ , is calculated by the following formula ([2]):

$$Q_{\alpha,well} = WI \frac{\rho_\alpha k_{r\alpha}}{\mu_\alpha} (p_b - p_\alpha - \gamma_\alpha g(z_{bh} - z)), \quad (52)$$

where  $WI$  is the well index. In CMG STARS, well rate can be calculated using unweighted method,

$$Q_{\alpha,well} = WI (p_b - p_\alpha - \gamma_\alpha g(z_{bh} - z)), \quad (53)$$

where  $WI$  is user input value. A well index defines the relationship among a well bottom hole pressure, a flow rate and a grid block pressure.  $p_b$  is the bottom hole pressure defined at the reference depth  $z$ ,  $z_{bh}$  is the depth of the perforation in grid cell, and  $p_\alpha$  is the phase pressure in grid block  $m$ . Well index can be read from modelling file and it can also be calculated using analytical method. For a vertical well, it can be defined as:

$$WI = \frac{2\pi h_3 \sqrt{k_{11} k_{22}}}{\ln(\frac{r_e}{r_w}) + s}, \quad (54)$$

where  $r_e$  is equivalent radius, and its calculation details can be read from [40] and CMG STARS manual. Horizontal can be defined similarly. We should mention that well modeling is the most complicated part in reservoir simulations and various operation constraints can be defined, such as fixed bottom hole pressure, fix liquid and gas rate constraints and thermal constraints. More details will be given in the numerical section, including more control methods and their mathematical models.

### 3 Numerical Methods

In our previous work, a few reservoir simulators and their numerical methods have been reported [21, 32, 34, 33]. The simulators share similar methods, such as time discretization scheme, spatial discretization scheme, decoupling method, linear solver and preconditioners [21]. For the sake of completeness, the numerical methods are introduced in this section.

#### 3.1 Time Discretization

Let  $u$  be a vector function,  $u^n$  be the solution of  $u$  at a given time step  $n$ , and  $F$  be non-linear mathematical system of thermal reservoir model. The backward Euler method is applied to discretize a time derivative,

$$\left(\frac{\partial u}{\partial t}\right)^{n+1} = \frac{u^{n+1} - u^n}{\Delta t} = F(u^{n+1}, t^{n+1}), \quad (55)$$

where  $\Delta t$  is a time step. An implicit non-linear system is obtained, which is solved at each time step using Newton method.

#### 3.2 Spatial Discretization

When fluids move in a reservoir, there may be fluid exchange in two neighboring grid blocks, which is described by transmissibility. Assuming  $d$  ( $d = x, y, z$ ) is a space direction and  $A$  be the area of a face in the  $d$  direction, the transmissibility  $K_{\alpha,d}$  for phase  $\alpha$  ( $\alpha = o, w, g$ ) is defined as

$$T_{\alpha,d} = \frac{KA}{\Delta d} \times \frac{K_{r\alpha}}{\mu_\alpha} \rho_\alpha, \quad (56)$$

where  $\Delta d$  is the grid block length in the  $d$  direction,  $K$  is the absolute permeability,  $K_{r\alpha}$  is the relative permeability of phase  $\alpha$ ,  $\mu_\alpha$  is the viscosity of phase  $\alpha$  and  $\rho_\alpha$  is the molar density of phase  $\alpha$ . The transmissibility is defined on each face of a grid block. If a face is internal face shared by two grid blocks, its value is the same for these two blocks. If the face is a boundary face, the transmissibility is zero, as the no-flow boundary condition is applied. Different weighting schemes must be applied to average different properties at an interface. The left part,  $\frac{KA}{\Delta d}$ , is geometric properties, and the harmonic averaging method is applied. The right part,  $\frac{K_{r\alpha}}{\mu_\alpha} \rho_\alpha$ , relies on fluid properties, and the upstream averaging method is applied [63]. The upstream finite difference method is employed to discretize the model.

#### 3.3 Linear Solver

The Jacobian matrix from Newton method is highly ill-conditioned, and the Krylov subspace solvers are applied to solve the linear system  $Ax = b$ . The key to an effective solution method is to choose a proper preconditioner  $M$ , which should be easy to setup and effective. In our previous work, a family of scalable CPR-like methods [21] have been developed for reservoir simulations, which have been applied to black oil model, compositional, in-situ combustion and the general thermal model in this paper. The unknowns are numbered grid block by grid block and the resulted matrix in each iteration is block-wise,

$$A = \begin{pmatrix} A_{11} & \cdots & \cdots & A_{1n} \\ A_{21} & A_{22} & \cdots & A_{2n} \\ \cdots & \cdots & \cdots & \cdots \\ A_{n1} & A_{n2} & \cdots & A_{nn} \end{pmatrix}, \quad (57)$$

where each sub-matrix  $A_{ij}$  is a square matrix.

#### 3.4 Decoupling Methods

A proper decoupling method is critical to the success of the CPR preconditioner. In general, the decoupling method is applied before applying the CPR preconditioner, which converts the original linear system to an equivalent linear system,

$$(D^{-1}A)x = D^{-1}b. \quad (58)$$

Several decoupling methods have been proposed, such as Quasi-IMPES, True-IMPES [60], Alternate Block Factorization (ABF) [61], full row sum (FRS) and dynamic row sum (DRS) [62] methods. The idea of ABF method is simple, which is defined as,

$$D_{abf} = \text{diag}(A_{11}, A_{22}, \cdots, A_{nn}). \quad (59)$$



It converts the block diagonal part to identity matrix. The FRS decoupling method is described as,

$$D_{frs}^{-1} = \text{diag}(D_1, D_2, \dots, D_n), \quad (60)$$

where,

$$D_i = \begin{pmatrix} 1 & 1 & \cdots & 1 \\ 0 & 1 & \cdots & 0 \\ \cdots & \cdots & \cdots & \cdots \\ 0 & \cdots & 1 & 0 \\ 0 & 0 & 0 & 1 \end{pmatrix}. \quad (61)$$

The diagonal part and the first row are 1 and all other locations are 0, which means to add the all rows to the first row. The DFS decoupling method is a simplified version of the FRS method, and details can be read in [62].

The Gauss-Jordan elimination (Gauss elimination, GJE) method has been used to solve linear systems. Its idea is to convert  $[D|A|b]$  to an equivalent linear system  $[I|\tilde{A}|\tilde{b}]$  by Gauss-Jordan elimination method, and the  $\tilde{b}$  is final solution. In this paper, it is adopted as a decoupling method and is applied grid block by grid block to turn the diagonal matrices to identity matrix. Pivoting technique is used and only row reordering is involved. Since the decoupling is processed block by block, no communication is required, which is friendly to parallel computing. The GJE decoupling is more efficient than the ABF method, which requires to calculate the inverse of the diagonal part and the matrix-matrix multiplications for each sub-matrix.

When the CPR-like preconditioners are applied to reservoir simulations, it is important to keep the pressure matrix positive definite. FRS method helps to enhance this property, from which the CPR-like preconditioners can benefit. A two-stage decoupling methods are also introduced. During the first stage, FRS and ABF methods are applied in sequence, which is noted as FRS-ABF decoupling method. And FRS and GJE methods are used as following stage, which is noted as FRS-GJE method. The FRS and DRS can also be applied as first stage decoupling, and then the ABF and the GJE methods can be applied as the second stage. In this case, two-stage decoupling methods are developed.

### 3.5 Preconditioners

Several scalable CPR-like preconditioner have been proposed [21], such as CPR-FP, CPR-PF, CPR-FPF, and CPR-FFPF methods. According to our practices, the CPF-FPF method, which is a three-stage preconditioner, is effective for black oil model and thermal model. It is described by Algorithm 1, where the first step is to solve an approximate solution using restricted additive Schwarz (RAS) method, the third step is to solve the subproblem by algebraic multi-grid method (AMG), the fifth step is to get an approximate solution again using restricted additive Schwarz method, and the second step and the forth step are to calculate residual.

It is well-known that the RAS method and AMG method are scalable for parallel computing, so the CPR-FPF method is also scalable. Here we should also mention that the setup phase of the parallel AMG method is computationally intense. For small model or easy model, the RAS method should work well too. The sub-problem for each CPU from RAS method is solved by ILUT by default, which can also be solved by ILU(k) or block ILU(k) [21].

---

#### Algorithm 1 The CPR-FPF Method

---

- 1:  $y = RAS(A)^{-1}f$
  - 2:  $y = y + \Pi_p AMG(A_{PP})^{-1} \Pi_r r$
  - 3:  $y = RAS(A)^{-1}f$
- 

The design and implementation details of the linear solver and preconditioners can be found in [54]. The thermal simulator and some other reservoir simulators base on the in-house platform, PRSI [55], which provides gridding, DOF (degrees of freedom), mapping, solver and preconditioner, well modeling, keyword parsing, option parsing, visualization, parallel input and output through MPI-IO, memory management, and communication management. The platform is implemented by C and utilizes MPI for communications. It is highly scalable and previous studies have shown that the platform and in-house simulators have ideal scalability using 4096 CPU cores. Details can be read from [55].

## 4 Numerical Studies

Numerical experiments are presented here, which includes a few sections. The first section validates our results against CMG STARS, which is the most widely applied thermal simulator. The purpose is to prove the correctness of our numerical methods, models and implementation. The second section tests the scalability of our thermal simulator using some giant models.

### 4.1 Validation

### 4.2 Heavy Oil

**Example 1** *The grid dimension of the model is  $9 \times 9 \times 4$ , with sizes of 29.17 ft, 29.17 ft and 10 ft in  $x$ ,  $y$  and  $z$  direction. Details of the model are presented in Table 1 to Table 5. Water component and one heavy oil component are simulated. As shown by Figure 1, the water-oil relative permeability and the liquid-gas relative permeability have sharp change. It has five vertical wells: one injection well in the center (5, 5), and four production wells in four corners, (1, 1), (1, 9), (9, 1) and (9, 9). The bottom hole pressure of the injection well, water rate and oil rate of each well are shown from Figure 2 to Figure 12. All results are compared with CMG STARS.*

Initial condition	
$k_{x,y,z}$ (md)	313, 424, 535
$\phi$	0.3
$\phi_c$	5e-4
$p$ (psi)	75
$T$ ( $^{\circ}F$ )	125
$S_{w,o,g}$	0.45, 0.55, 0.

Table 1: Input data for Example 1

Properties	H2O	HO
$M$ (lb/lbmole)	18	600
$p_{crit}$ (psi)	3206.2	
$T_{crit}$ ( $^{\circ}F$ )	705.4	
$\rho_{ref}$ (lbmole/ft <sup>3</sup> )	3.464	0.10113
$cp$ (1/psi)	3.999e-6	5.e-6
$ct1$ (1/ $^{\circ}F$ )	4e-4	3.8e-4
$cpg1$ (Btu/( $^{\circ}F \cdot lbmol$ ))	7.613	300
$cpg2$ (Btu/( $^{\circ}F^2 \cdot lbmol$ ))	8.616e-4	0
$hvr$ (Btu/( $^{\circ}F^{ev} \cdot lbmol$ ))	1657	
$ev$	0.38	
$avg$ (cp/ $^{\circ}F$ )	1.13e-5	
$bvg$	1.075	
$avisc$ (cp)	0.0047352	2
$bvisc$ ( $^{\circ}F$ )	2728.2	5728.2
$kv1$ (psi)	1.7202e6	0
$kv4$ ( $^{\circ}F$ )	-6869.59	0
$kv5$ ( $^{\circ}F$ )	-376.64	0

Table 2: Input data for Example 1 (cont'd)

Figure 2 is the bottom hole pressure of the injection well. Figure 3 is the water production rate of the first production well. Figure 4 is the water production rate of the second production well. Figure 5 is the water production rate of the third production well. Figure 6 is the water production rate of the forth production well. Figure 7 is the total water production rate of all production wells. Figure 8 is the oil production rate of the first production well. Figure 9 is the oil production

$S_w$	$k_{rw}$	$k_{row}$
0.45	0.0	0.4
0.47	0.000056	0.361
0.50	0.000552	0.30625
0.55	0.00312	0.225
0.60	0.00861	0.15625
0.65	0.01768	0.1
0.70	0.03088	0.05625
0.75	0.04871	0.025
0.77	0.05724	0.016
0.80	0.07162	0.00625
0.82	0.08229	0.00225
0.85	0.1	0.0

Table 3: Input data for Example 1 (cont'd).

$S_l$	$k_{rg}$	$k_{rog}$
0.45	0.2	0.0
0.55	0.14202	0.0
0.57	0.13123	0.00079
0.60	0.11560	0.00494
0.62	0.10555	0.00968
0.65	0.09106	0.01975
0.67	0.08181	0.02844
0.70	0.06856	0.04444
0.72	0.06017	0.05709
0.75	0.04829	0.07901
0.77	0.04087	0.09560
0.80	0.03054	0.12346
0.83	0.02127	0.15486
0.85	0.01574	0.17778
0.87	0.01080	0.20227
0.90	0.00467	0.24198
0.92	0.00165	0.27042
0.94	0.0	0.30044
1.	0.0	0.4

Table 4: Input data for Example 1 (cont'd).

rate of the second production well. Figure 10 is the oil production rate of the third production well. Figure 11 is the oil production rate of the forth production well. Figure 12 is the total oil production rate of all production wells. All figures show that our results match CMG STARS very well, which confirms our methods and implementation are correct.

### 4.3 Heavy Oil and Light Oil

**Example 2** *This model is similar as Example 1 except that a light oil component is added and the well operations are changed. It has five vertical wells: one injection well in the center (5, 5), and four production wells in four corners, (1, 1), (1, 9), (9, 1) and (9, 9). The bottom hole pressure of the injection well, water rate and oil rate of each well are shown from Figure 13 to Figure 28. All results are compared with CMG STARS.*

Figure 13 is the bottom hole pressure of the injection well. Figure 14 is the water production rate of the first production well. Figure 15 is the water production rate of the second production well. Figure 16 is the water production rate of the third production well. Figure 17 is the water production rate of the forth production well. Figure 18 is the total water production rate of all production wells. Figure 19 is the gas production rate of the first production well. Figure 20 is the gas production rate of the second production well. Figure 21 is the gas production rate of the third production well. Figure 22 is the gas

Well conditions		
Injector	water ( <i>bbl/day</i> )	100
	wi ( <i>ft · md</i> )	1e4
	tinjw ( <i>°F</i> )	450
	steam quality	0.4
Producer 1	bhp ( <i>psi</i> )	17
	wi ( <i>ft · md</i> )	1e4
	steamtrap ( <i>°F</i> )	10
Producer 2	bhp ( <i>psi</i> )	17
	wi ( <i>ft · md</i> )	1e4
	steamtrap ( <i>°F</i> )	20
Producer 3	bhp ( <i>psi</i> )	17
	wi ( <i>ft · md</i> )	1e4
	steamtrap ( <i>°F</i> )	30
Producer 4	bhp ( <i>psi</i> )	17
	wi ( <i>ft · md</i> )	1e4
	steamtrap ( <i>°F</i> )	40

Table 5: Input data for Example 1 (cont'd).

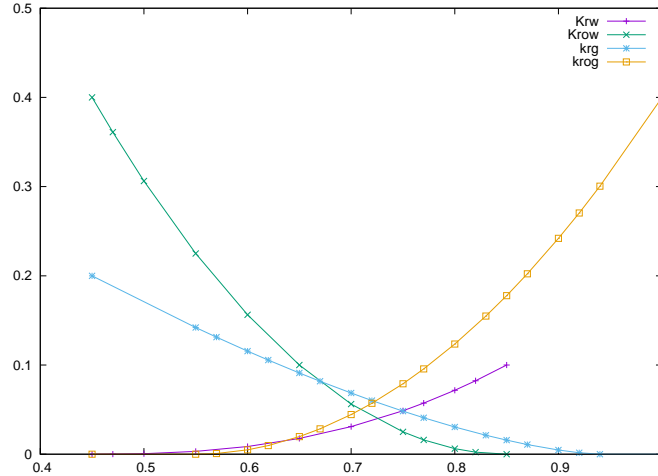


Figure 1: Example 1: relative permeability of the water-oil table and liquid-gas table)

Initial condition	
$k_{x,y,z}$ ( <i>md</i> )	313, 424, 535
$\phi$	0.3
$\phi_c$	5e-4
$p$ ( <i>psi</i> )	4000
$T$ ( <i>°F</i> )	125
$S_{w,o,g}$	0.45, 0.55, 0.
$x$	0.6, 0.4

Table 6: Input data for Example 1

production rate of the forth production well. Figure 23 is the total gas production rate of all production wells. Figure 24 is the oil production rate of the first production well. Figure 25 is the oil production rate of the second production well. Figure 26 is the oil production rate of the third production well. Figure 27 is the oil production rate of the forth production well. Figure 28 is the total oil production rate of all production wells. All figures show that our results match CMG STARS very well, which confirms our methods and implementation are correct.

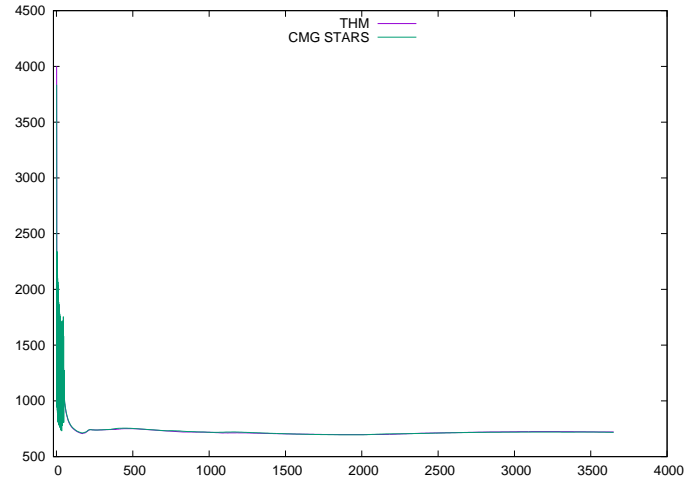


Figure 2: Example 1: injection well, bottom hole pressure (psi)

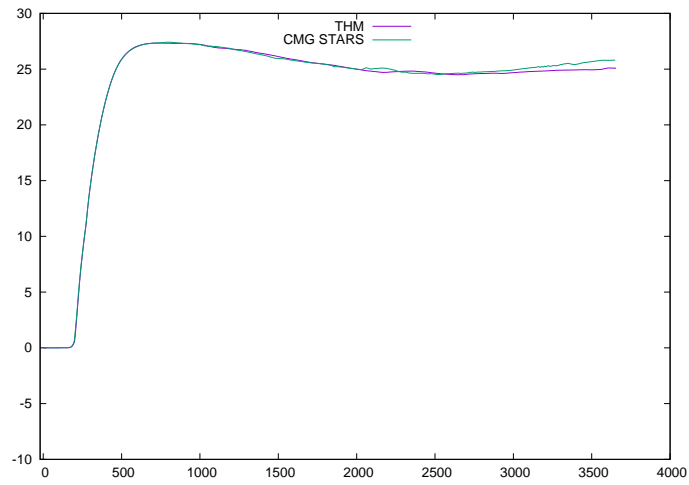


Figure 3: Example 1: water production rate (bbl/day), first production well

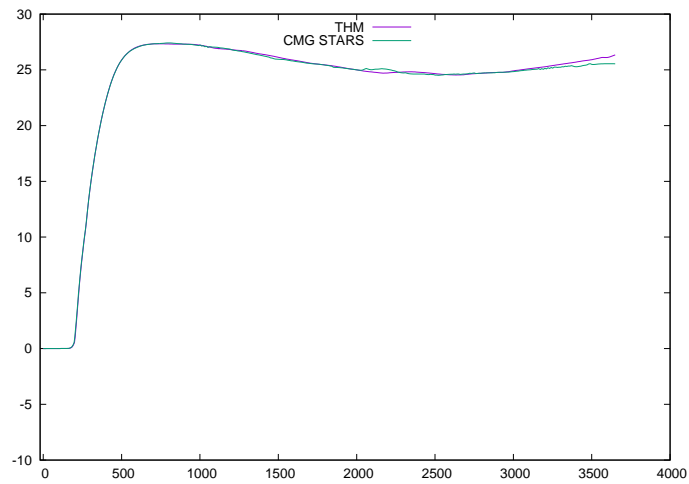


Figure 4: Example 1: water production rate (bbl/day), second production well

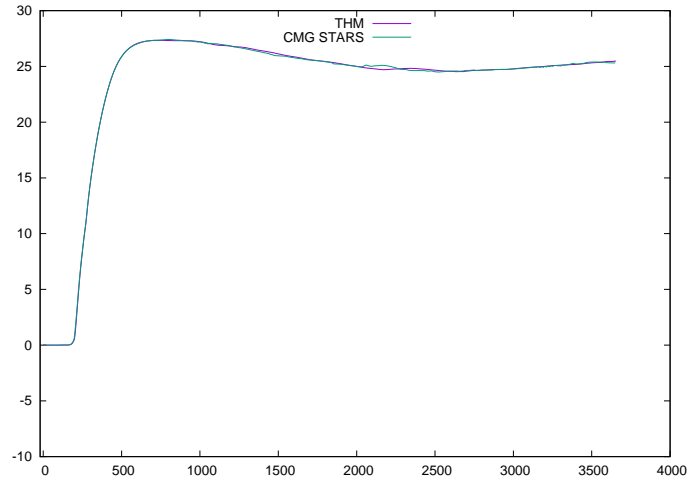


Figure 5: Example 1: water production rate (bbl/day), third production well

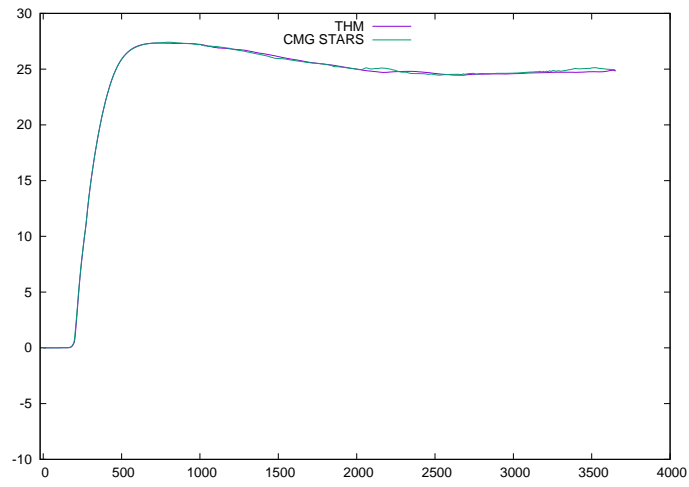


Figure 6: Example 1: water production rate (bbl/day), forth production well

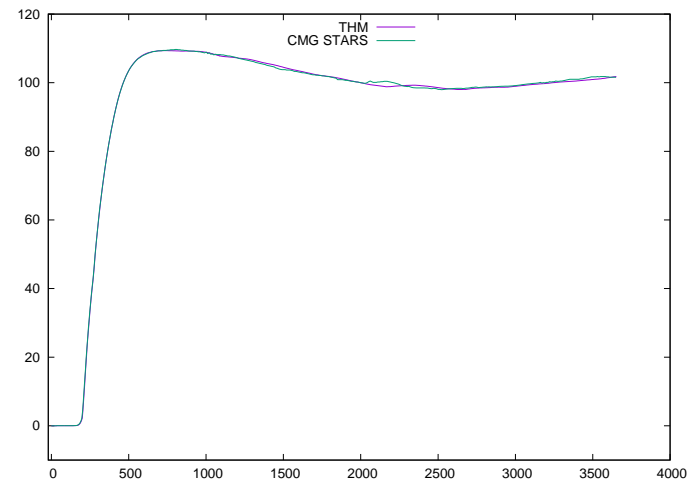


Figure 7: Example 1: total water production rate (bbl/day)

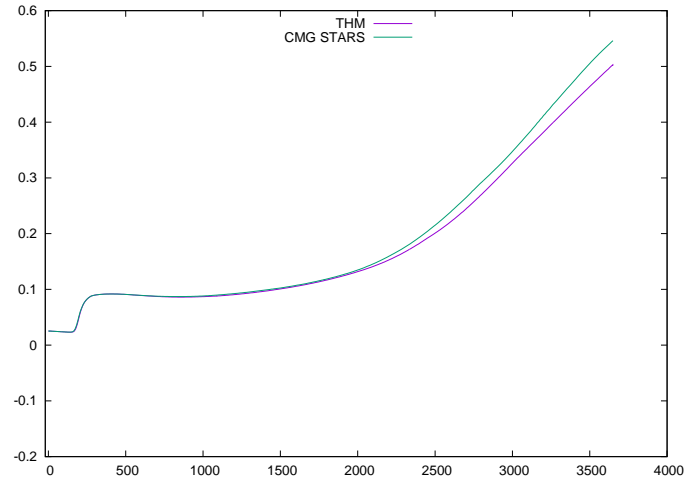


Figure 8: Example 1: oil production rate (bbl/day), first production well

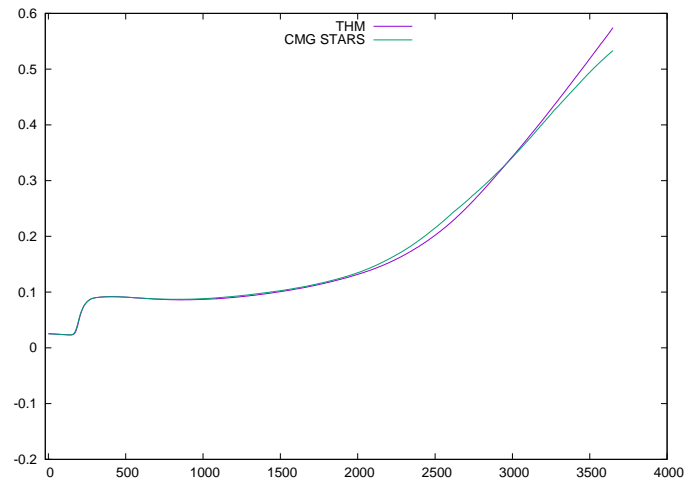


Figure 9: Example 1: oil production rate (bbl/day), second production well

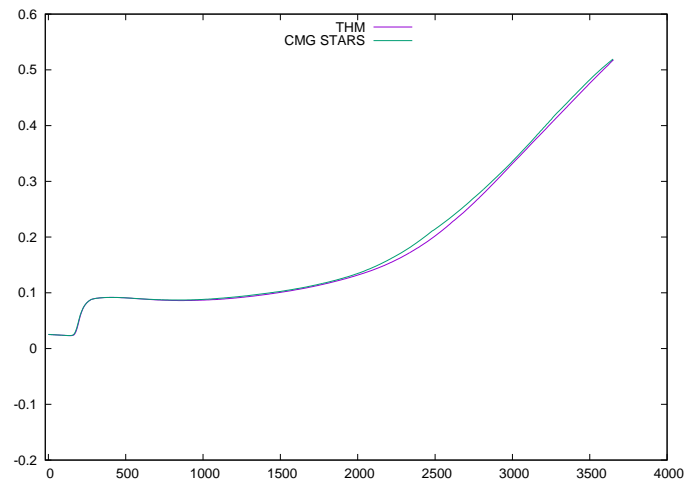


Figure 10: Example 1: oil production rate (bbl/day), third production well

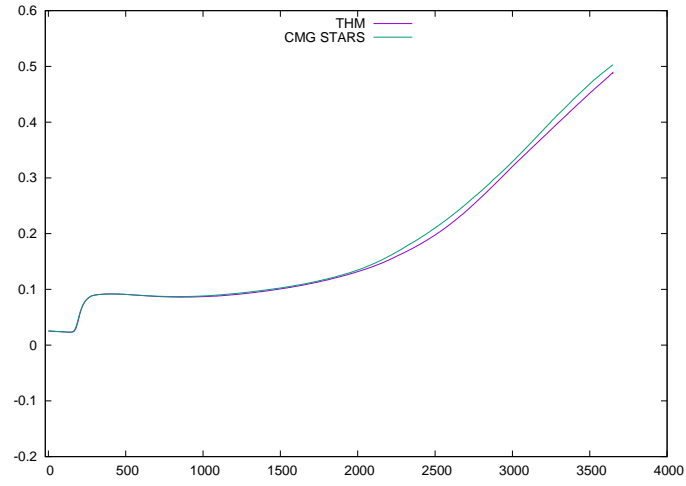


Figure 11: Example 1: oil production rate (bbl/day), forth production well

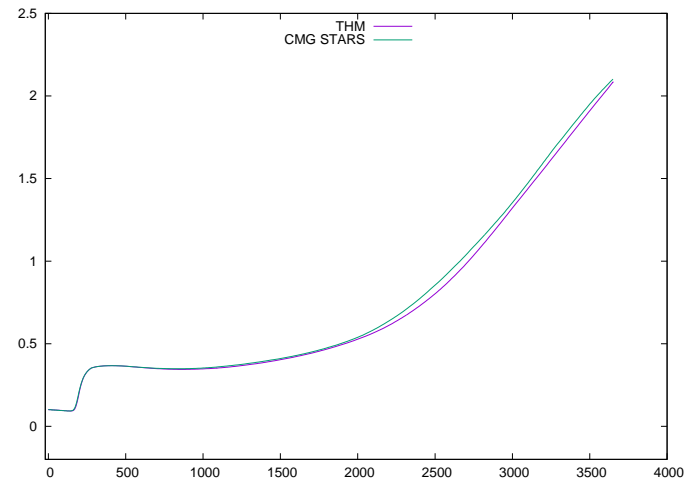


Figure 12: Example 1: total oil production rate (bbl/day)

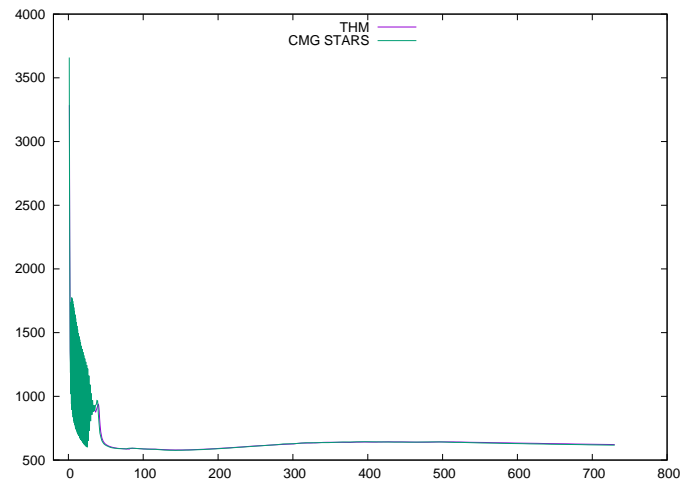


Figure 13: Example 2: injection well, bottom hole pressure (psi)



Properties	LO
$M$ (lb/lbmole)	250
$p_{crit}$ (psi)	225
$T_{crit}$ ( $^{\circ}F$ )	800
$\rho_{ref}$ (lbmole/ft <sup>3</sup> )	0.2092
$cp$ (1/psi)	5.e-6
$ct1$ (1/ $^{\circ}F$ )	3.8e-4
$cpg1$ (Btu/( $^{\circ}F \cdot lbmol$ ))	247.5
$hvr$ (Btu/( $^{\circ}F^{ev} \cdot lbmol$ ))	657
$ev$	0.38
$avg$ ( $cp/^{\circ}F$ )	5.e-5
$bvg$	0.9
$avisc$ ( $cp$ )	0.287352
$bvisc$ ( $^{\circ}F$ )	3728.2
$kv1$ (psi)	7.9114e4
$kv4$ ( $^{\circ}F$ )	-1583.71
$kv5$ ( $^{\circ}F$ )	-446.78

Table 7: Input data for Example 2

Well conditions		
Injector	water (bbl/day)	100
	wi (ft · md)	1e4
	tinjw ( $^{\circ}F$ )	450
	steam quality	0.3
Producer 1	bhp (psi)	17
	wi (ft · md)	2e4
Producer 2	bhp (psi)	17
	wi (ft · md)	3e4
Producer 3	bhp (psi)	17
	wi (ft · md)	4e4
Producer 4	bhp (psi)	17
	wi (ft · md)	5e4

Table 8: Input data for Example 2 (cont'd).

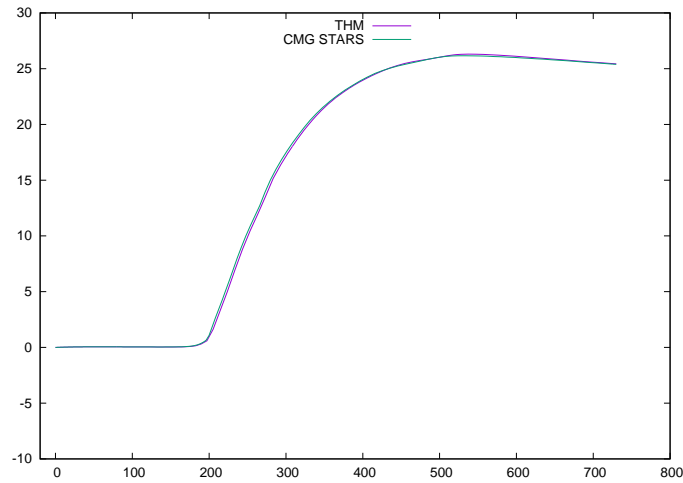


Figure 14: Example 2: water production rate (bbl/day), first production well

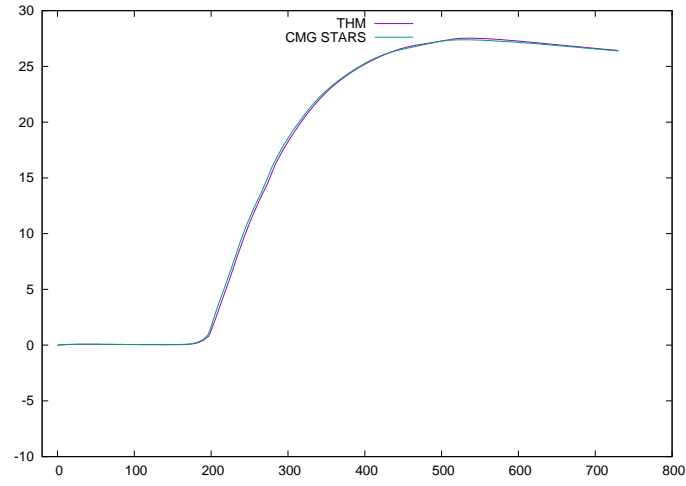


Figure 15: Example 2: water production rate (bbl/day), second production well

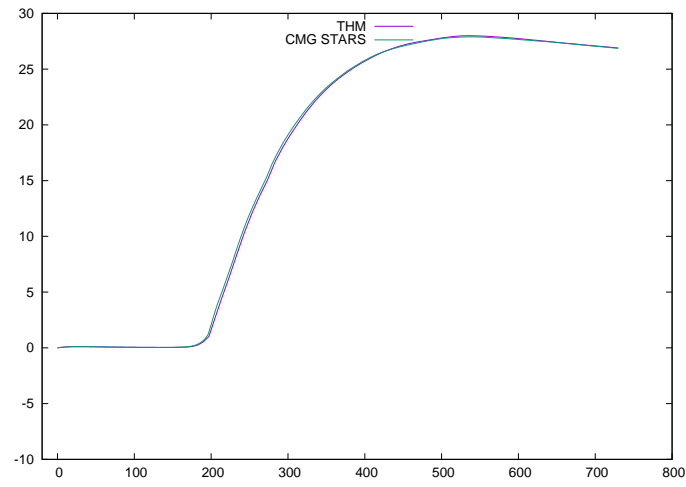


Figure 16: Example 2: water production rate (bbl/day), third production well

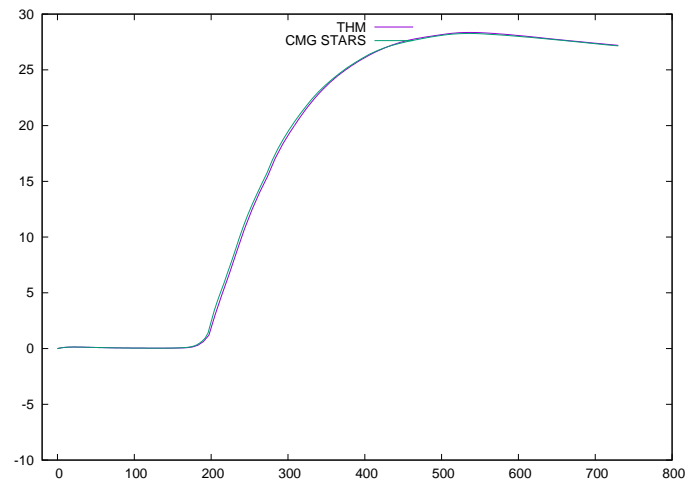


Figure 17: Example 2: water production rate (bbl/day), fourth production well

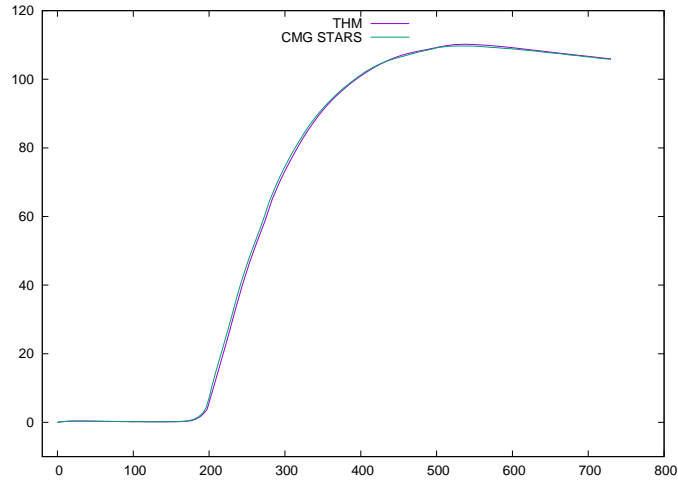


Figure 18: Example 2: total water production rate (bbl/day)

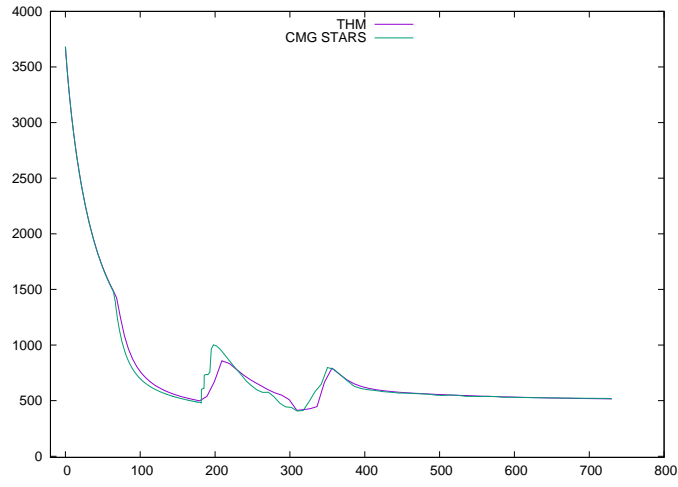


Figure 19: Example 2: gas production rate ( $ft^3/day$ ), first production well

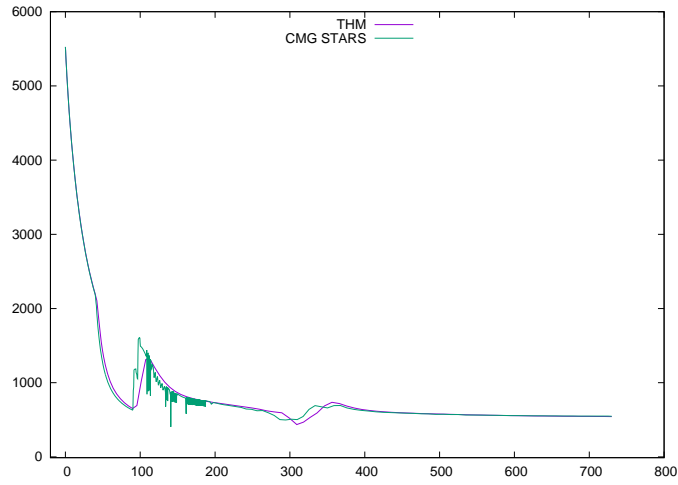


Figure 20: Example 2: gas production rate ( $ft^3/day$ ), second production well

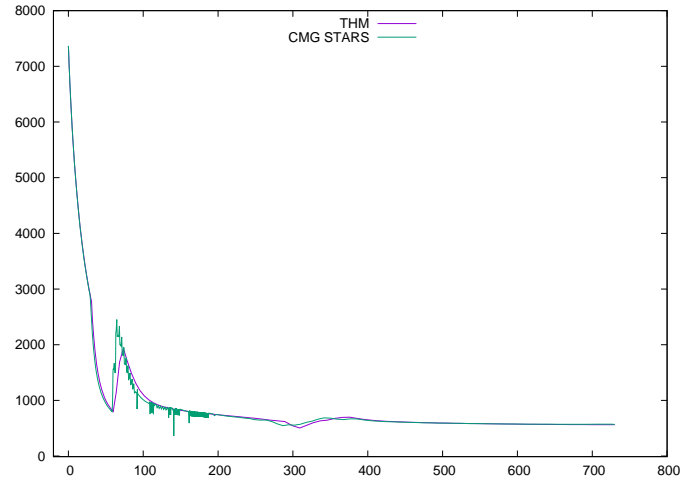


Figure 21: Example 2: gas production rate ( $ft^3/day$ ), third production well

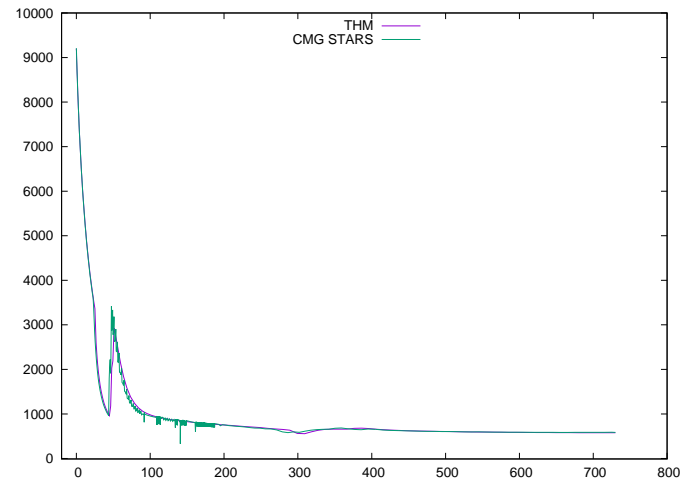


Figure 22: Example 2: gas production rate ( $ft^3/day$ ), forth production well

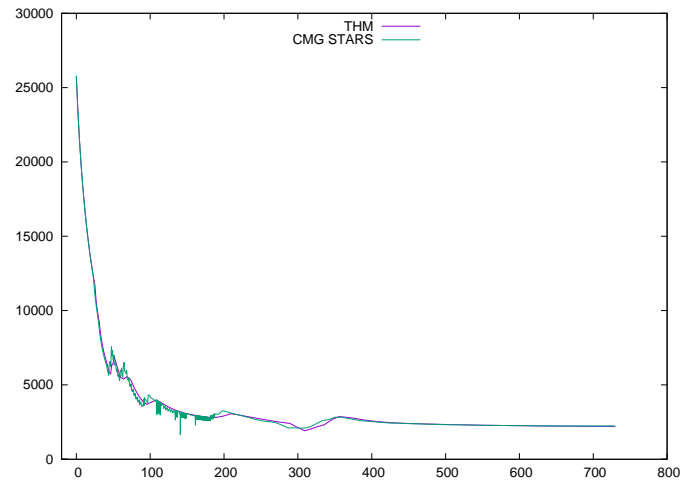


Figure 23: Example 2: total gas production rate ( $ft^3/day$ )

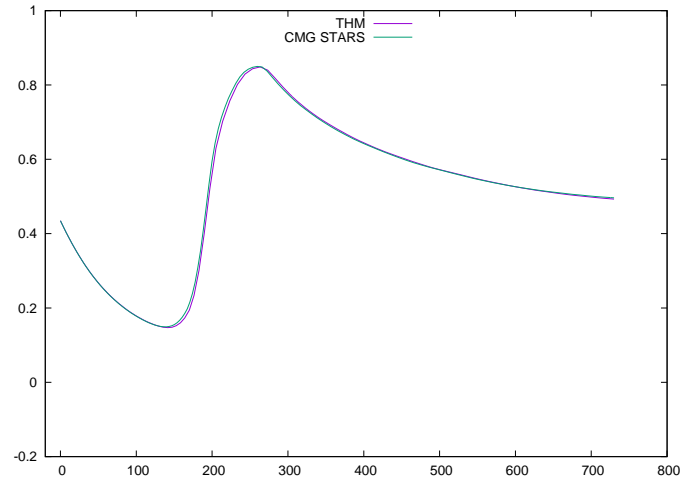


Figure 24: Example 2: oil production rate (bbl/day), first production well

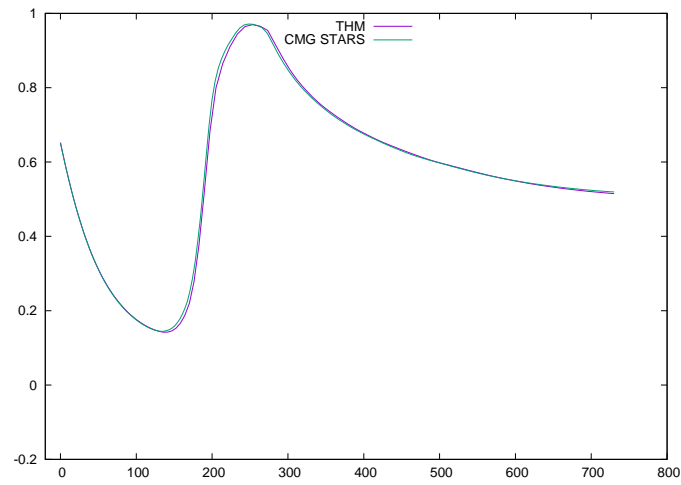


Figure 25: Example 2: oil production rate (bbl/day), second production well

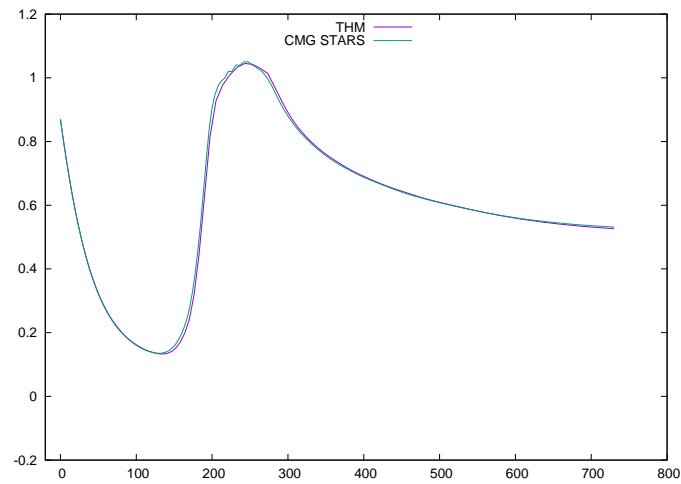


Figure 26: Example 2: oil production rate (bbl/day), third production well

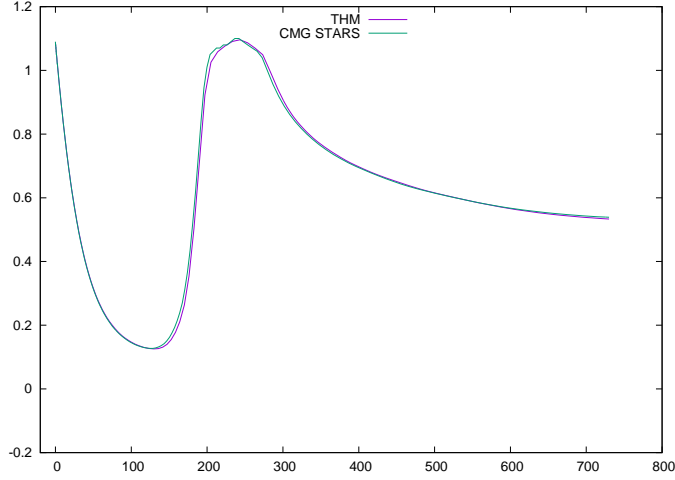


Figure 27: Example 2: oil production rate (bbl/day), forth production well

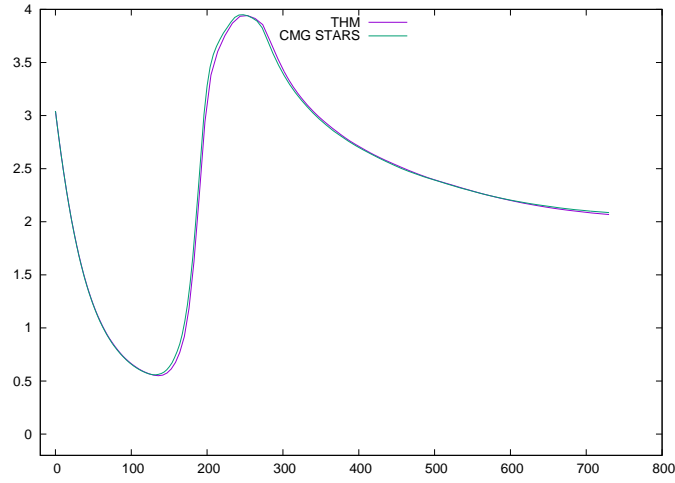


Figure 28: Example 2: total oil production rate (bbl/day)

#### 4.4 Non-condensable Gas

**Example 3** This model is similar as Example 2 except that two non-condensable gas oil components are added. Data is provided in Table 9 ad Table 9. It also has five vertical wells: one injection well in the center (5, 5), and four production wells in four corners, (1, 1), (1, 9), (9, 1) and (9, 9). The bottom hole pressure of the injection well, water rate and oil rate of each well are shown from Figure 29 to Figure 44. All results are compared with CMG STARS.

Initial condition	
$k_{x,y,z}$ (md)	313, 424, 535
$\phi$	0.3
$\phi_c$	5e-4
$p$ (psi)	4000
$T$ ( $^{\circ}F$ )	125
$S_{w,o,g}$	0.4, 0.5, 0.1
$x$	0.6, 0.4
$y$	4.73644e-4, 0, 0.486126, 0.2, 0.3134

Table 9: Input data for Example 1

Properties	N2	Isert
$M$ (lb/lbmole)	28	40.8
$p_{crit}$ (psi)	730	500
$T_{crit}$ ( $^{\circ}F$ )	-181	-232
$cpg1$ (Btu/( $^{\circ}F \cdot lbmol$ ))	6.713	7.44
$cpg2$ (Btu/( $^{\circ}F \cdot lbmol$ ))	-4.883e-7	-0.0018
$cpg3$ (Btu/( $^{\circ}F \cdot lbmol$ ))	1.287e-6	1.975e-6
$cpg4$ (Btu/( $^{\circ}F \cdot lbmol$ ))	-4.36e-10	-4.78e-10
$avg$ (cp/ $^{\circ}F$ )	2.1960e-4	2.1267e-4
$bvg$	0.721	0.702

Table 10: Input data for Example 3

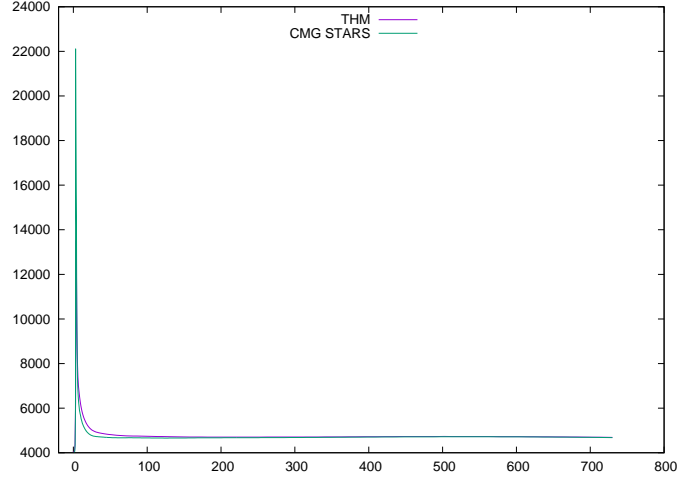


Figure 29: Example 3: injection well, bottom hole pressure (psi)

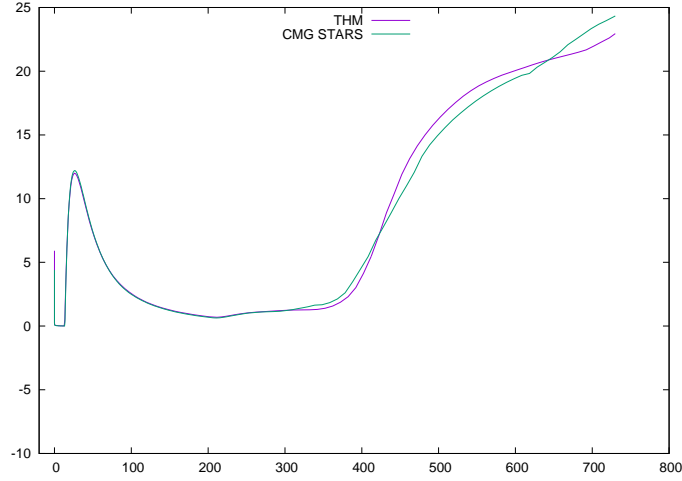


Figure 30: Example 3: water production rate (bbl/day), first production well

Figure 29 is the bottom hole pressure of the injection well. Figure 30 is the water production rate of the first production well. Figure 31 is the water production rate of the second production well. Figure 32 is the water production rate of the third production well. Figure 33 is the water production rate of the forth production well. Figure 34 is the total water production rate of all production wells. Figure 35 is the gas production rate of the first production well. Figure 36 is the gas production rate of the second production well. Figure 37 is the gas production rate of the third production well. Figure 38 is the gas production rate of the forth production well. Figure 39 is the total gas production rate of all production wells. Figure 40 is

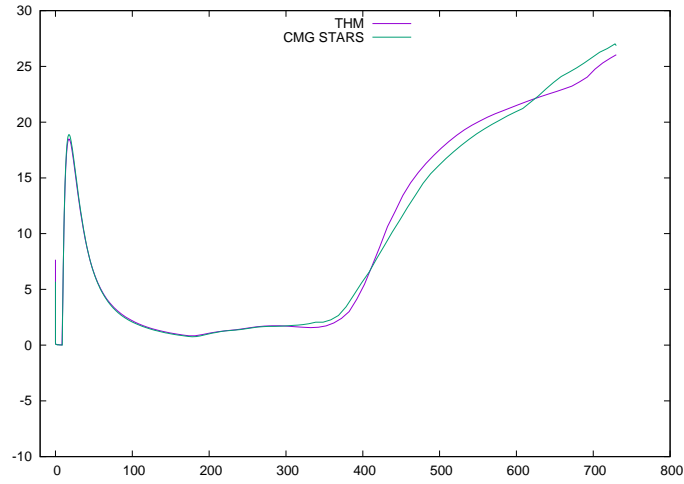


Figure 31: Example 3: water production rate (bbl/day), second production well

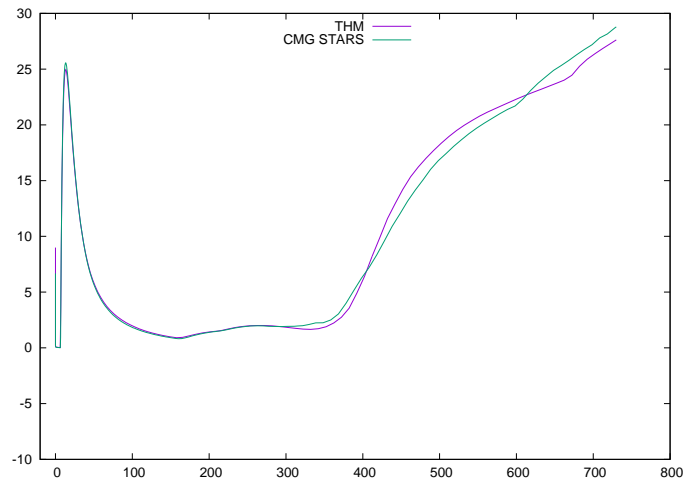


Figure 32: Example 3: water production rate (bbl/day), third production well

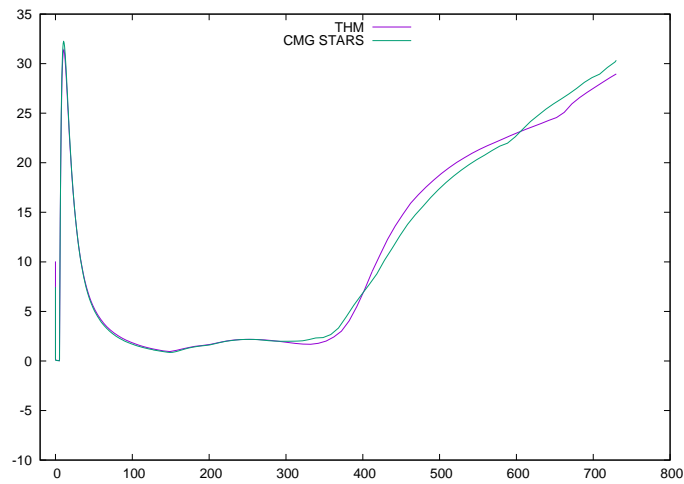


Figure 33: Example 3: water production rate (bbl/day), forth production well



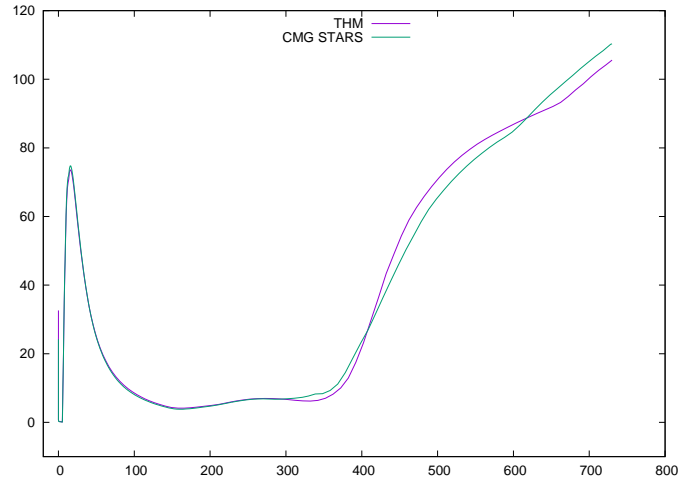


Figure 34: Example 3: total water production rate (bbl/day)

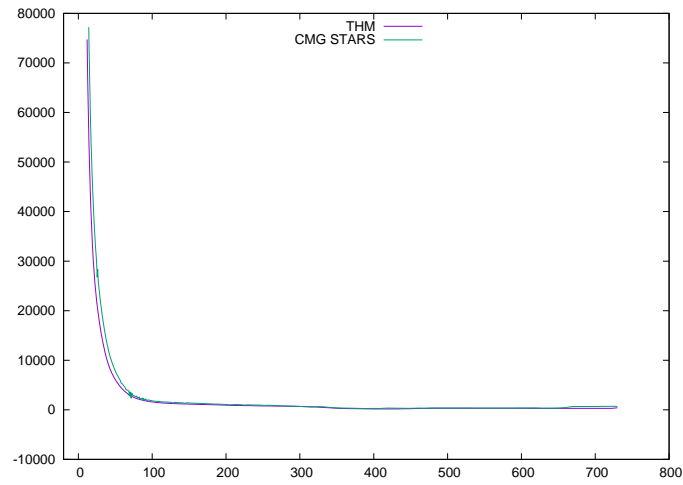


Figure 35: Example 3: gas production rate ( $ft^3/day$ ), first production well

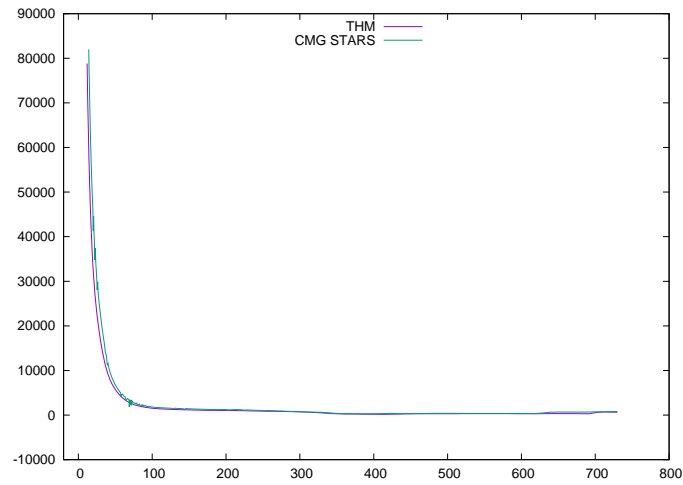


Figure 36: Example 3: gas production rate ( $ft^3/day$ ), second production well

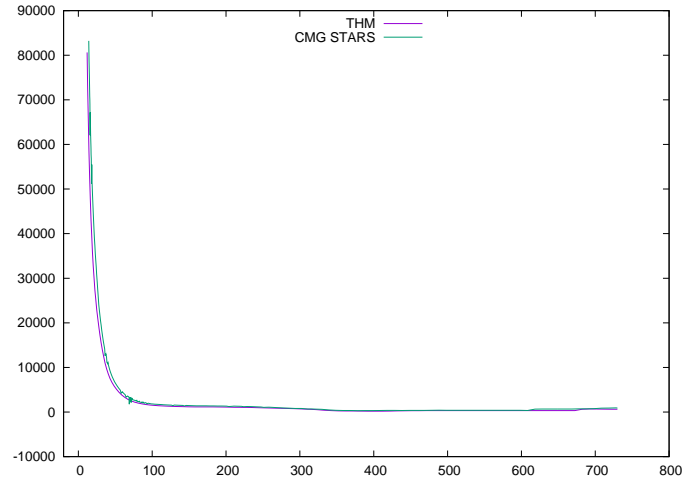


Figure 37: Example 3: gas production rate ( $ft^3/day$ ), third production well

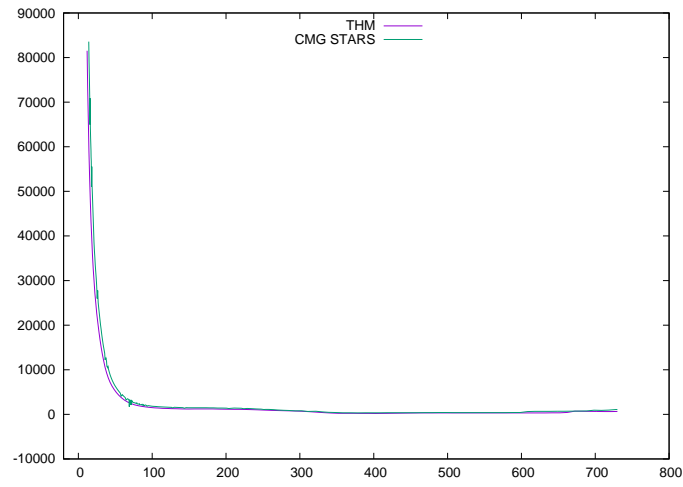


Figure 38: Example 3: gas production rate ( $ft^3/day$ ), forth production well

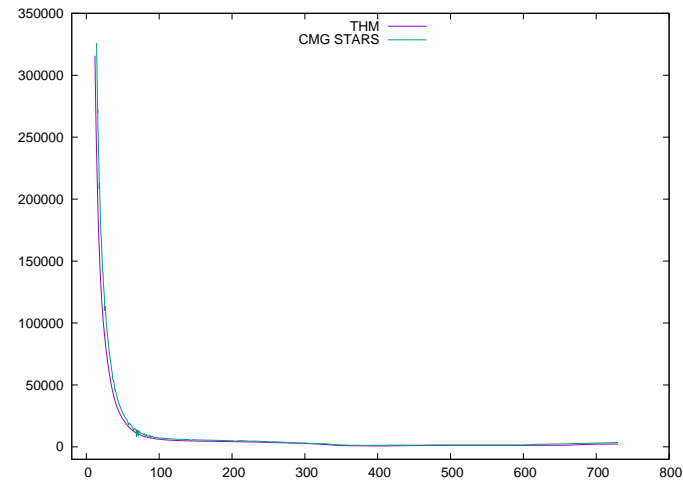


Figure 39: Example 3: total gas production rate ( $ft^3/day$ )

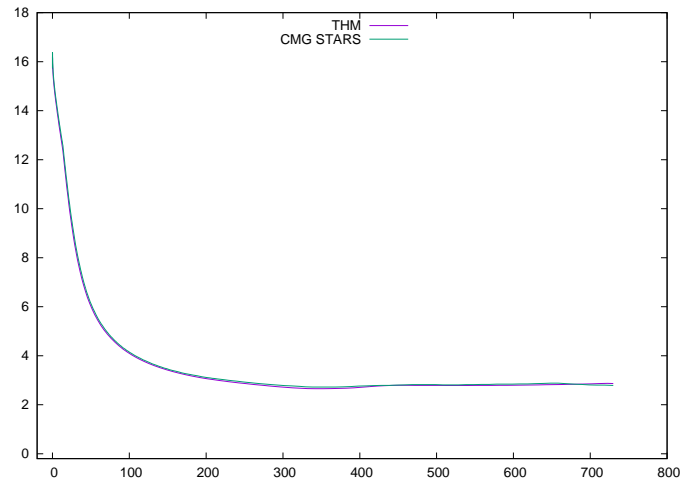


Figure 40: Example 3: oil production rate (bbl/day), first production well

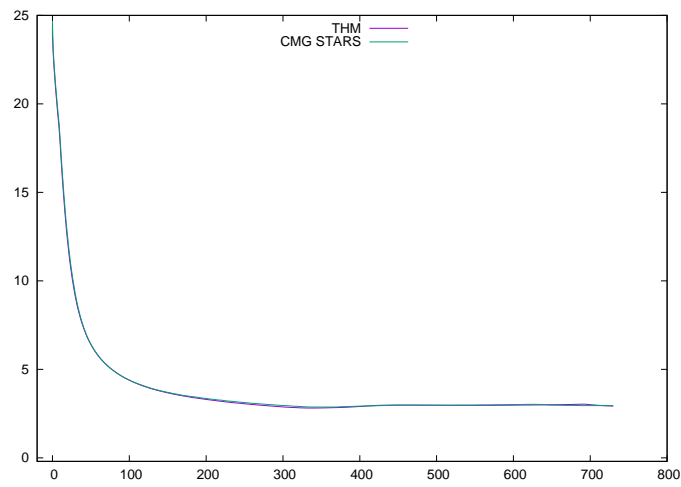


Figure 41: Example 3: oil production rate (bbl/day), second production well

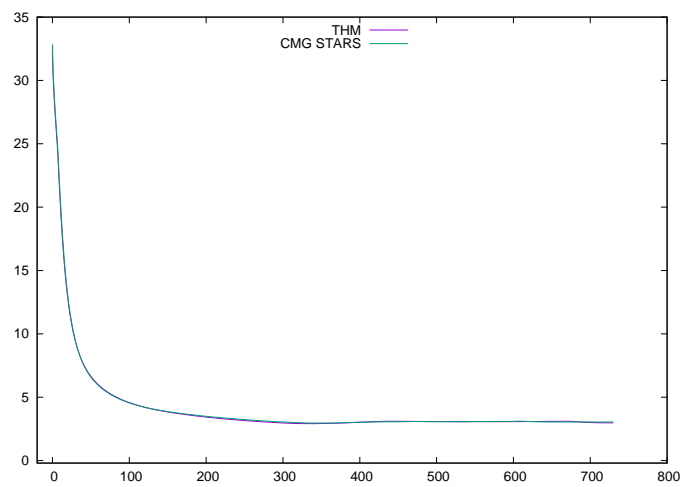


Figure 42: Example 3: oil production rate (bbl/day), third production well

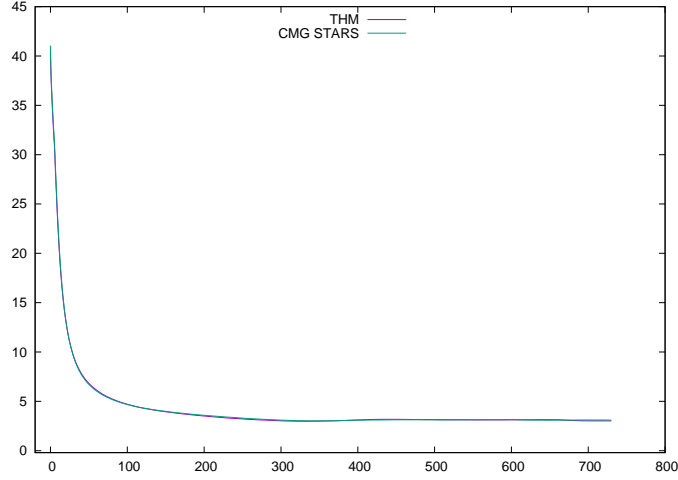


Figure 43: Example 3: oil production rate (bbl/day), forth production well

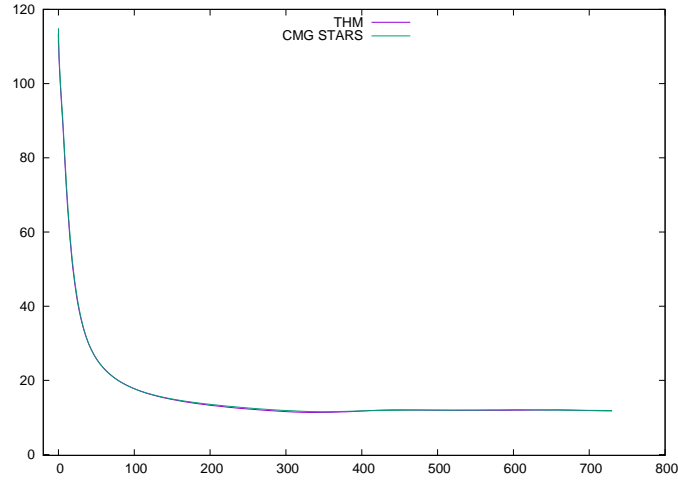


Figure 44: Example 3: total oil production rate (bbl/day)

the oil production rate of the first production well. Figure 41 is the oil production rate of the second production well. Figure 42 is the oil production rate of the third production well. Figure 43 is the oil production rate of the forth production well. Figure 44 is the total oil production rate of all production wells. All figures show that our results match CMG STARS very well, which confirms our methods and implementation are correct.

#### 4.5 Well Controls

The water (steam) injection rate, water production and oil production rates, bottom hole pressure for each well are reported. All rates are surface rates, and flash calculations are required to convert reservoir rates to surface rates. The injection rate is measured as cold water equivalent. As we mentioned, the well modeling is the most complicated, and we will change well operation constraints to test our simulator.

If there is no special statement, the non-linear method is the standard Newton method with a tolerance  $1e-6$  and maximal iterations of 10, the linear solver is BICGSTAB with a tolerance  $1e-4$  and maximal iterations of 100, and the preconditioner is CPR-FPF method. All wells use implicit numerical methods, though the explicit method has been implemented.

#### 4.5.1 Fixed Bottom Hole Pressure

When the fixed bottom hole pressure condition is applied to a well, the well equation is written as,

$$p_b = c, \quad (62)$$

where  $c$  is pressure and is a constant. The property calculations for production wells are straightforward. However, for injection well, iso-enthalpy flash calculation is required to determine the temperature and the density of the injected fluid in each well perforation.

**Example 4** *The injection well operates at 1500 psi. The steam quality is 0, and its temperature is 450 F. Two production wells operates are 17 psi. The simulation period is 365 days. Figure 45, 46, and 47 show the water injection rate, total water production and total oil production. The rates are surface rate. All results are compared with CMG STARS. From these figures, we can see that our results match CMG STARS.*

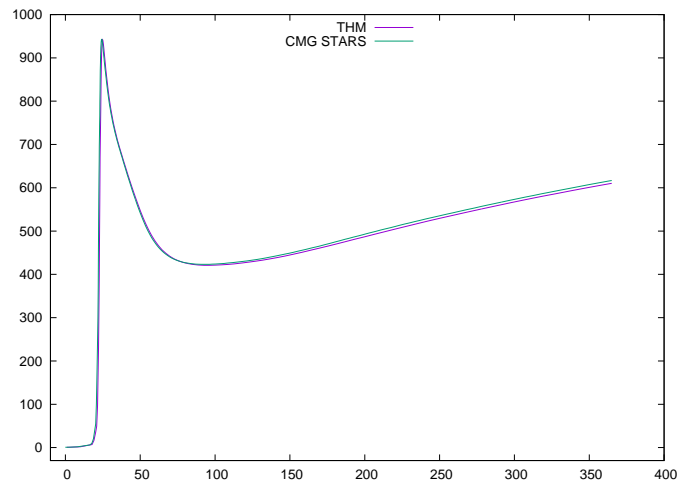


Figure 45: Example 4: water injection rate (bbl/day)

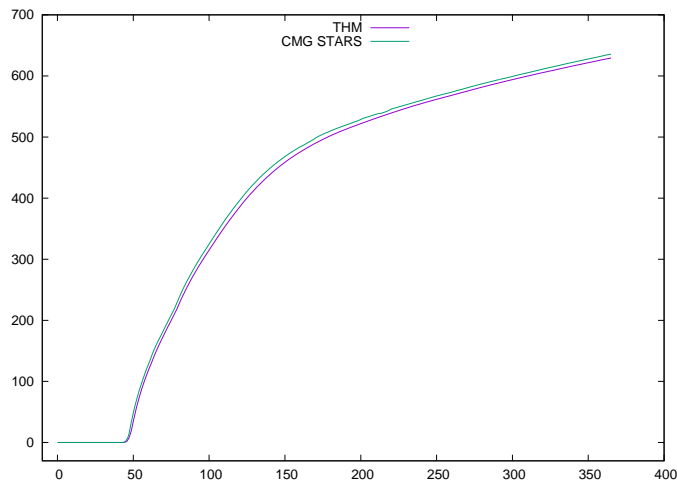


Figure 46: Example 4: water production rate (bbl/day)

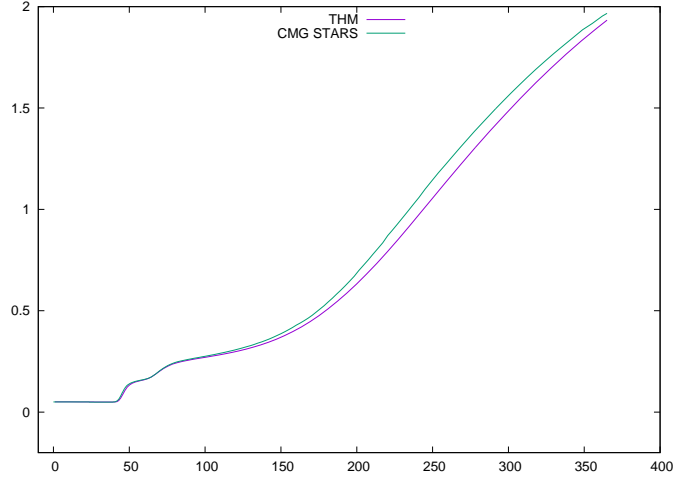


Figure 47: Example 4: oil production rate (bbl/day)

#### 4.5.2 Fixed Rate

Fixed rate constraints are commonly used, including fixed oil rate, fixed water rate, fixed gas rate, and fixed liquid rate (oil and water). The rate can be reservoir rate or surface rate. The volume of a fluid in reservoir condition can be obtained easily. However, the volume of a fluid in surface condition requires flash calculation to determine the distribution in oil, water and gas phases. In this section, the rates are surface volume rates. For phase  $\alpha$ , its fixed rate constraint is described by the following equation:

$$\sum_m (Q_{\alpha,well})_m = c, \quad (63)$$

where  $c$  is a constant rate and known. The fixed liquid rate is written as,

$$\sum_m (Q_{w,well})_m + \sum_m (Q_{o,well})_m = c, \quad (64)$$

**Example 5** *The injection well operates at 300 bbl/day, and the production wells operates at 17 psi. The simulation period is 365 days. Figure 48, 49, and 50 are bottom hole pressure for injection well, total water production and total oil production. All results are compared with CMG STARS.*

When fixed rate constraint is applied to a well, its rate is known, but its bottom hole pressure is unknown, which should be obtained by Newton methods. Figure 48 represents the bottom hole pressure of the injection well, from which we can see that our results match CMG STARS exactly. It means the methods and the implementation are correct. Figure 49 is the total water production rate, which also match CMG STARS exactly. Figure 50 is the total oil production rate (bbl/day). The results match CMG STARS exactly in the first 100 days, and after that, there is slight difference. The reason is that each simulator has its own numerical settings and automatical numerical tunings. For example, the density, bottom hole pressure update and mobility for wells in CMG STARS have many parameters to control, and CMG has automatical bottom hole pressure update algorithms depending on time step and pressure changes, whose details are unknown to us.

#### 4.5.3 Rate and Pressure Constraints

A well may have many operation constraints, such as maximal injection rate with maximal bottom hole pressure for injection well, maximal oil production rate with minimal bottom hole pressure for production well, and maximal liquid rate with minimal bottom hole pressure for production well.

**Example 6** *The injection well has a maximal injection rate of 200 bbl/day and a maximal bottom hole pressure of 1500 psi. The steam has a steam quality of 0.3 and temperature of 450 F. The first production well has a maximal liquid rate of 0.5 bbl/day and a minimal bottom hole pressure of 17 psi. The second production well has a maximal oil rate of 0.4 bbl/day and a minimal bottom hole pressure of 17 psi. The simulation period is 365 days. The bottom hole pressures for each well, water rates and oil rates for each well are presented from Figure 51 to Figure 59. All results are compared with CMG STARS.*

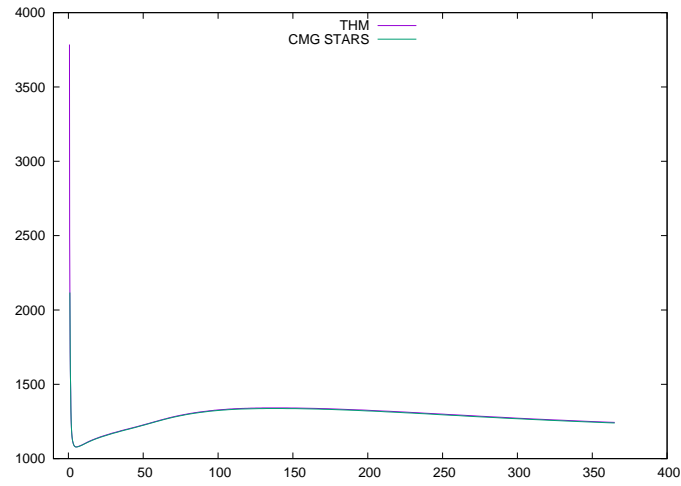


Figure 48: Example 5: injection well, bottom hole pressure (psi)

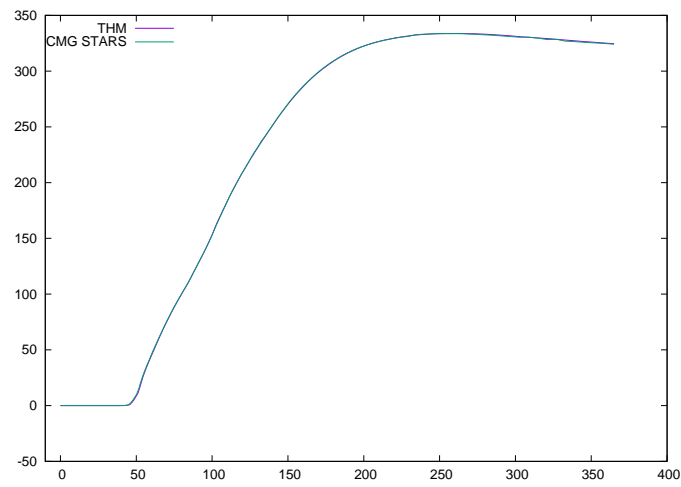


Figure 49: Example 5: water production rate (bbl/day)

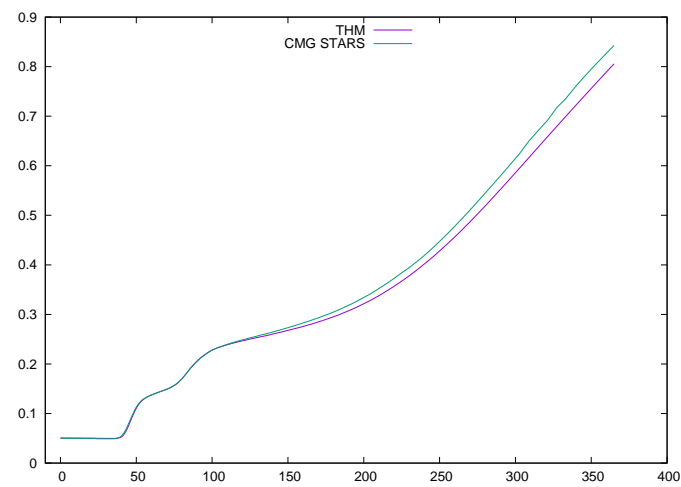


Figure 50: Example 5: oil production rate (bbl/day)

Figure 51, 52 and 53 show the bottom hole pressure for injection well and production wells. The results for production wells match well. Our Newton method shows good convergence but CMG STARS shows severe convergence issues. From Figure 54 to Figure 59, we can see that the water rate and oil rate for each well, total water rate and total oil rate match CMG STARS well.

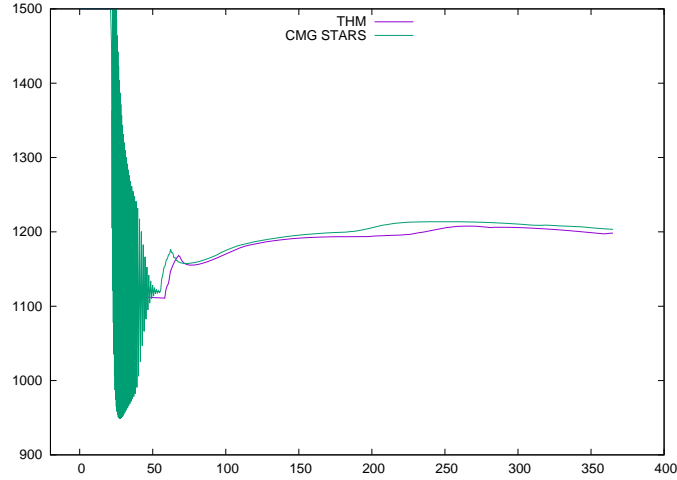


Figure 51: Example 6: injection well, bottom hole pressure (psi)

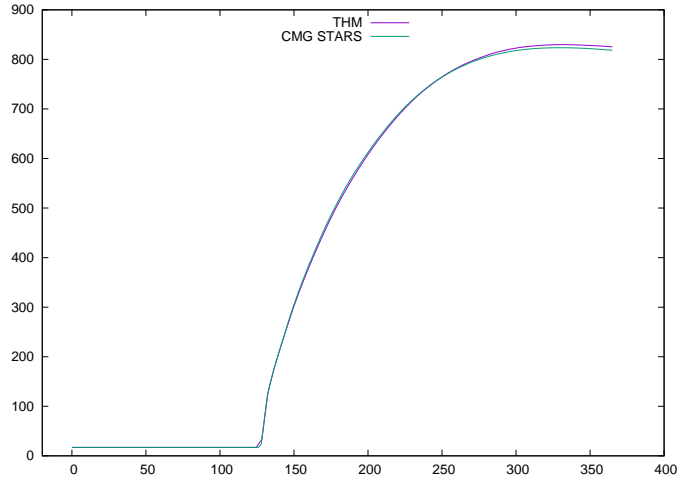


Figure 52: Example 6: first production well, bottom hole pressure (psi)

#### 4.5.4 Constant Heat Transfer Model

CMG STARS is the most popular thermal simulator, and it has many heater models, such as constant heat transfer model (`heatr` in CMG STARS), convective heat transfer model and heat well, which are applied to model heating stage. The first two types can be defined in any grid block. However, the heat well (`HTWELL` in CMG STARS) can only be defined in a real well, such as injection well and production well. The constant heat transfer model means at some grid blocks, there exist heat transfer at certain rate, such as 1,000 Btu/day. The energy exchange can occur in any grid block. The heat transfer can be turned on or off using schedule.

**Example 7** *In this example, the injection well operates at a fixed steam injection rate of 100 bbl/day, and the steam quality is 0 at a temperature of 450 F. Each production well operates at fixed bottom hole pressure of 17 psi. Constant heat transfers*



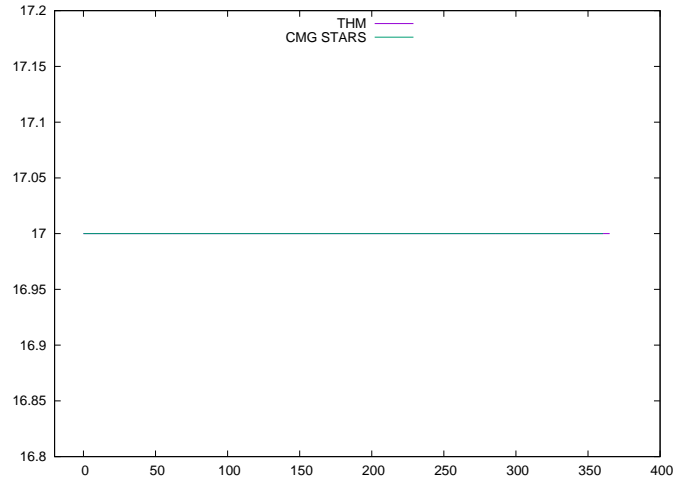


Figure 53: Example 6: second production well, bottom hole pressure (psi)

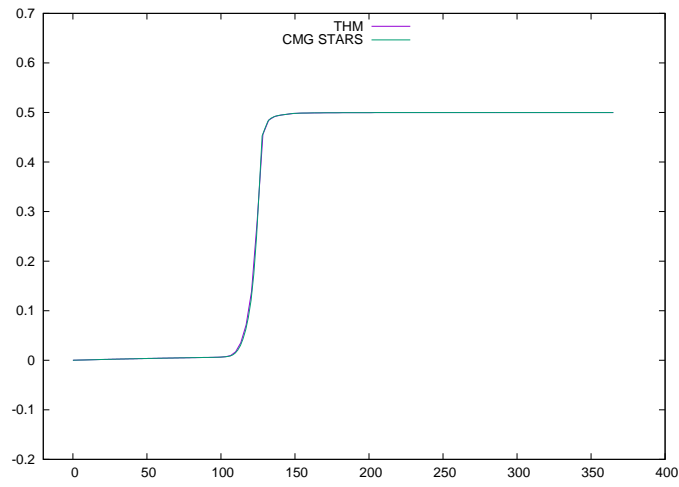


Figure 54: Example 6: water production rate (bbl/day), first production well

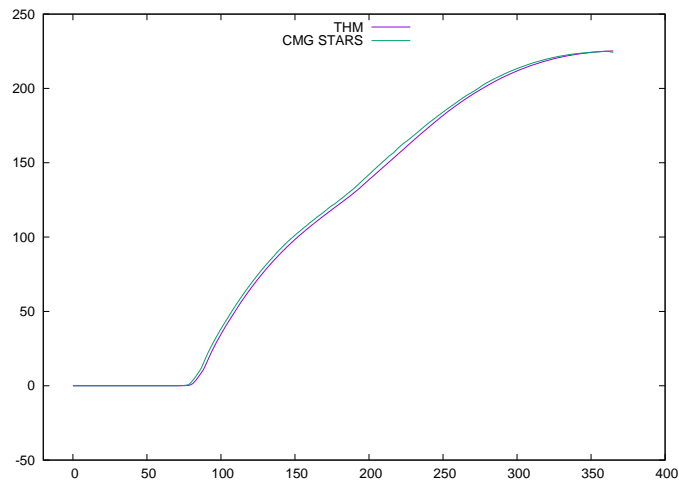


Figure 55: Example 6: water production rate (bbl/day), second production well

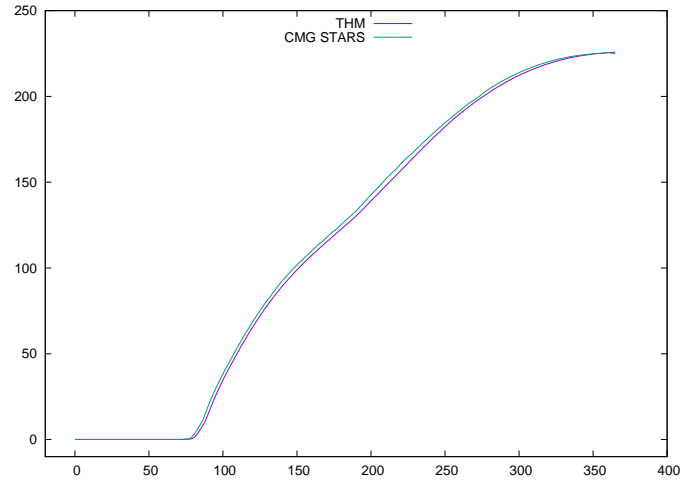


Figure 56: Example 6: total water production rate (bbl/day)

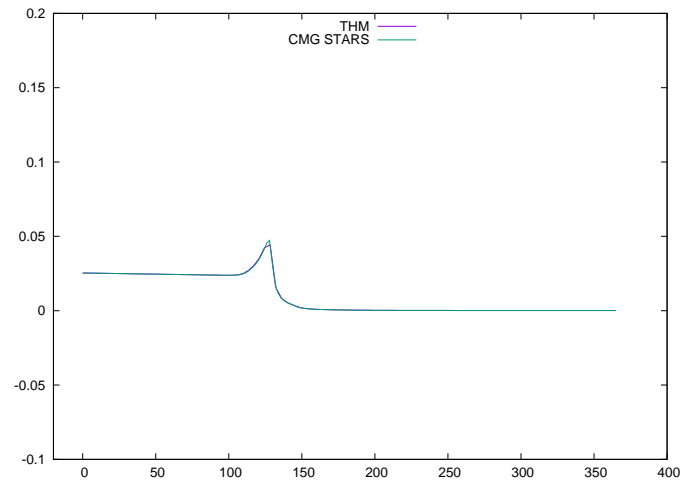


Figure 57: Example 6: oil production rate (bbl/day), first production well

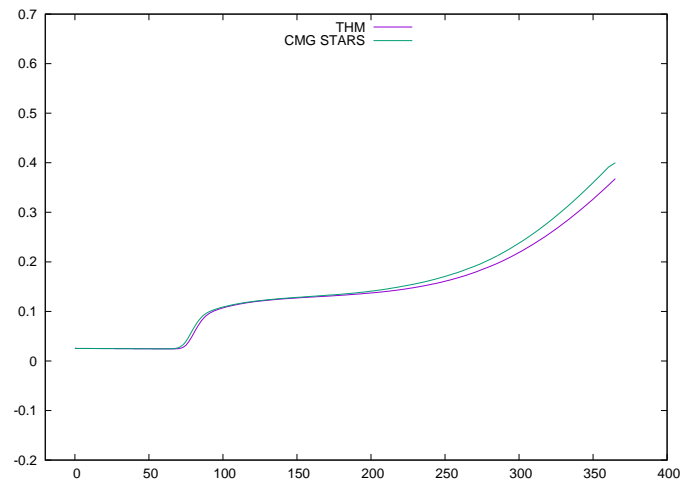


Figure 58: Example 6: oil production rate (bbl/day), second production well

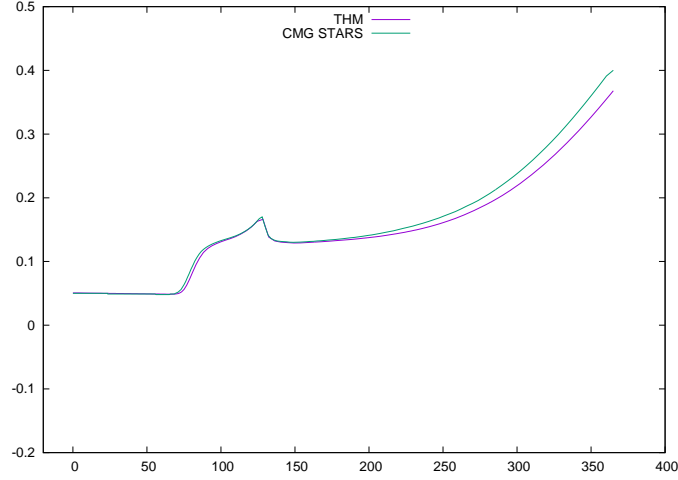


Figure 59: Example 6: total oil production rate (bbl/day)

to each perforation at a rate of  $1e6$  Btu/day. The simulation period is 365 days. Figure 60 to Figure 63 show simulated results and they are compared with CMG STARS.

Figure 60 is the bottom hole pressure and compared with CMG STARS. We can see that the match is exact. For injection rate shown by Figure 61, our convergence is smoother than CMG STARS. The water and oil production rates match very well as shown in Figure 63 and Figure 62.

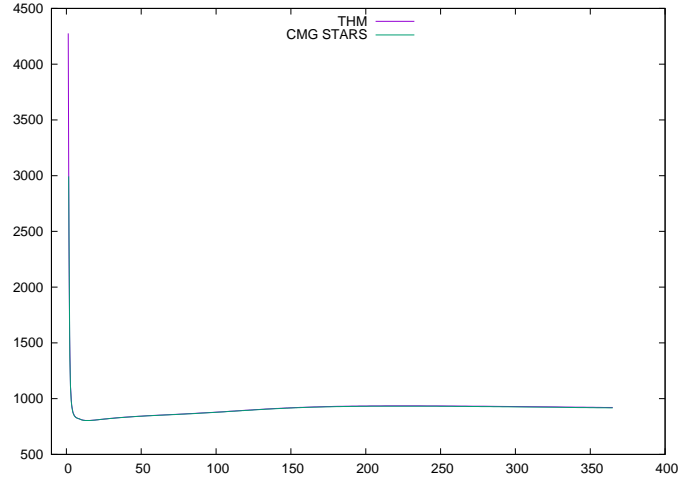


Figure 60: Example 7: injection well, bottom hole pressure (psi)

#### 4.5.5 Convective Heat Transfer Model

Constant heat transfer model simulates constant heat exchange while convective heat transfer model defines dynamic heat transfer, which is controlled by two parameters: **uhtr** (proportional heat transfer coefficient, Btu/day-F) and **tmpset** (temperature setpoint, F) (UHTR and TEMSET in CMG STARS). If **uhtr** is positive, it means to gain heat from source, the heat rate in a grid block is calculated as,

$$q = \begin{cases} \text{uhtr} * (\text{tmpset} - T), & \text{if } \text{tmpset} > T; \\ 0, & \text{if } \text{tmpset} \leq T; \end{cases} \quad (65)$$

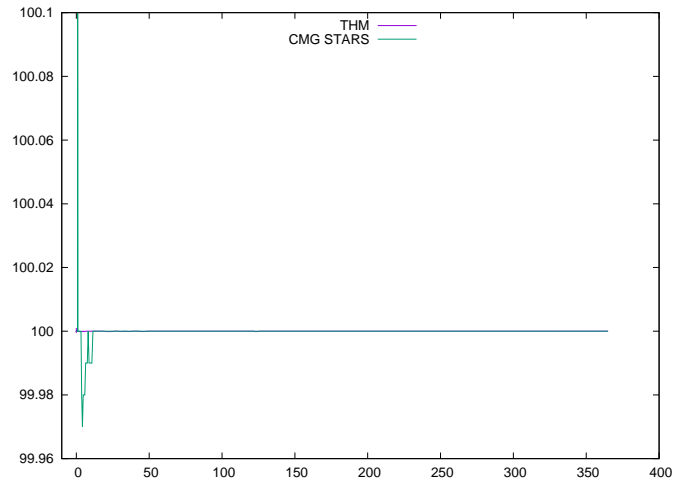


Figure 61: Example 7: water injection rate (bbl/day)

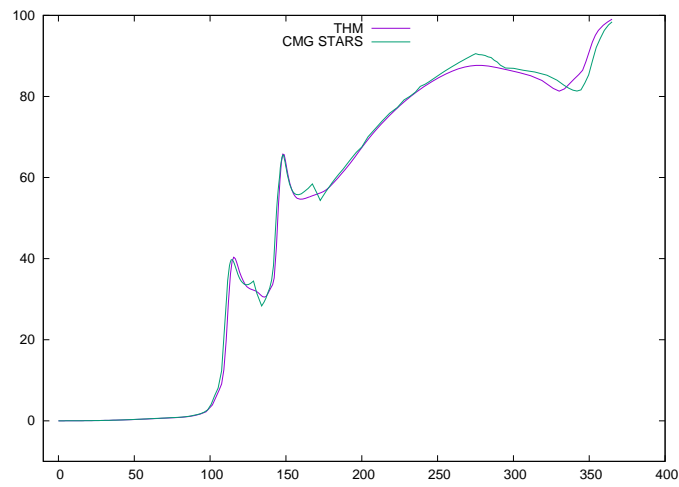


Figure 62: Example 7: water production rate (bbl/day)

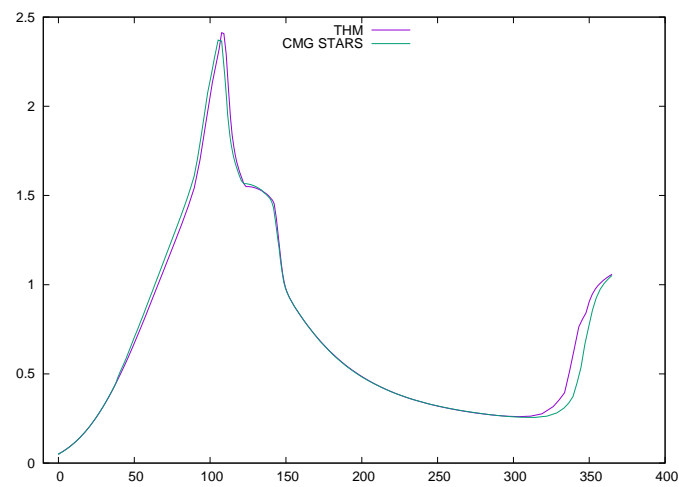


Figure 63: Example 7: oil production rate (bbl/day)

If  $\text{uhtr}$  is negative, it means the reservoir loses heat, the heat rate in a grid block is calculated as,

$$q = \begin{cases} \text{uhtr} * (T - \text{tmpset}), & \text{if } \text{tmpset} < T; \\ 0, & \text{if } \text{tmpset} \geq T; \end{cases} \quad (66)$$

where  $T$  is the reservoir temperature.

**Example 8** Here the injection rate is 50 bbl/day, and production wells have fixed bottom hole pressure. Each perforation of production wells have a  $\text{uhtr}$  of  $4e4$  btu/day-F and a temperature setpoint ( $\text{tmpset}$ ) of 500 F. Again the simulation period is 365 days. All results are compared with CMG STARS. Figure 64, 65, 66 and 67 are injection well bottom hole pressure, injection surface rate, water production surface rate and oil production surface rate. From these figures, we can see the match between our simulator and CMG STARS is excellent.

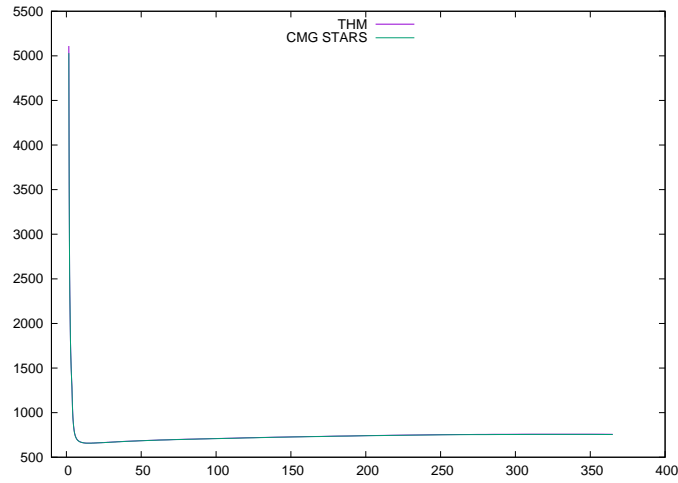


Figure 64: Example 8: injection well, bottom hole pressure (psi)

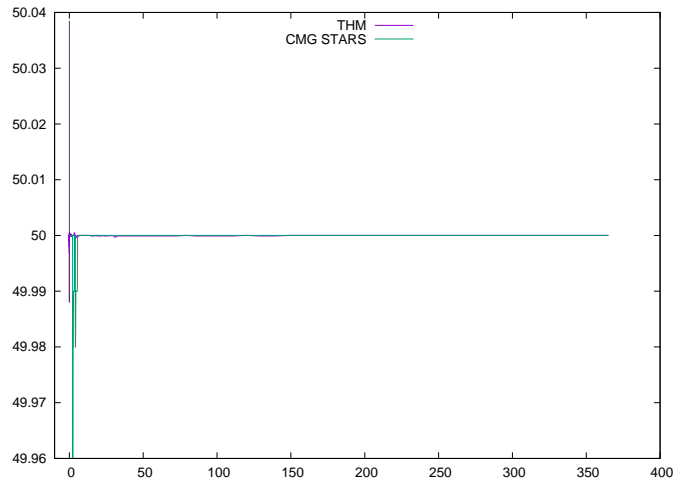


Figure 65: Example 8: water injection rate (bbl/day)

#### 4.5.6 Heater Well

As mentioned above, the constant and convective heat transfer models can be defined in any grid block. Another heat model is also developed in CMG STARS and our simulator, which is noted as HTWELL in CMG STARS. This type of heater is

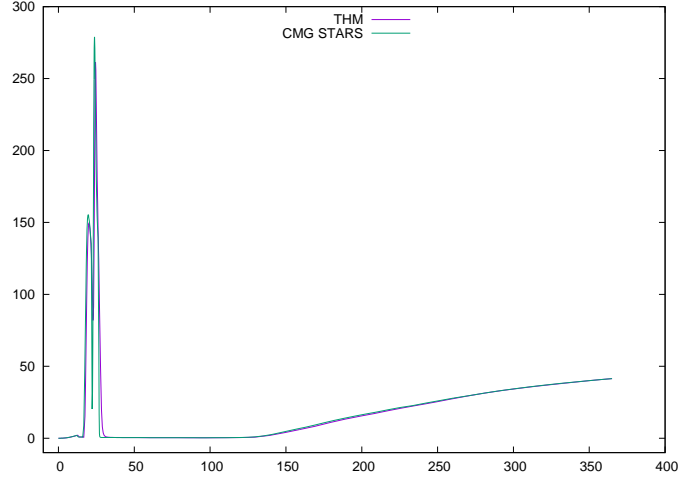


Figure 66: Example 8: water production rate (bbl/day)

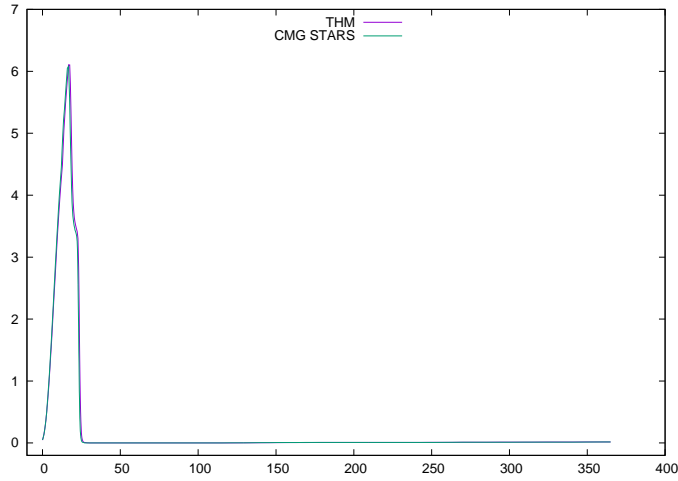


Figure 67: Example 8: oil production rate (bbl/day)

defined in a production or injection well, which has the same perforations as the well contains the heater well. This heater well is more complicated than constant and convective heater transfer models, which has more controls, such as heat rate model (HTWRATE or HTWRATEPL in CMG STARS), temperature model (HTWTEMP in CMG STARS), heat index model (HTWI in CMG STARS), and dual rate/temperature model. The dual rate/temperature model has two direction controls: uni-directed (UNIDIRECT in CMG STARS) and bi-directed (BIDIRECT in CMG STARS).

For heat rate control (model), the heat rate in a perforation  $m$  is calculated as,

$$q = q_{hspec} = Q_{hspec} L_m / L_w, \quad (67)$$

where  $q$  is the heat rate,  $Q_{hspec}$  is total heat rate defined by HTWRATE,  $L_m$  is the length of the layer well completion, and  $L_w$  is the total well length (sum of  $L_m$ ).

For temperature model, the heat rate in a perforation is calculated as,

$$q = q_{wspec} = I_m * (T_{wspec} - T_m), \quad (68)$$

where  $I_m$  is the heat index,  $T_{wspec}$  is specify wellbore temperature,  $T_m$  is grid block temperature. We should mention that there are two method for calculating heat conduct index: 1) use thermal conductivity formula introduced in mathematical model section; 2) use heat index introduced here (by turning HTWI on in CMG STARS). For heat index model, the user input well index or internal index can be converted to heat index.

When dual rate/temperature model is enabled, the rate model and temperature model are switched automatically. For heating ( $Q_{hspec} > 0$ ), the heat rate in a layer is defined as,

$$q = \min\{I_m * \Delta T_m, q_{hspec}\}, \quad (69)$$

where  $\Delta T_m$  is defined as,

$$\Delta T_m = \begin{cases} \max\{T_{wspec} - T_k, 0\}, & \text{for UNIDIRECT} \\ T_{wspec} - T_k, & \text{for BIDIRECT,} \end{cases} \quad (70)$$

The  $T_k$  is reservoir temperature in a grid block. The UNIDIRECT option shuts down heater when temperature difference is zero; while BIDIRECT allows heating and cooling (heat loss).

For cooling ( $Q_{hspec} < 0$ ), the heat rate in a layer is defined as,

$$q = \max\{I_m * \Delta T_m, q_{hspec}\}, \quad (71)$$

where  $\Delta T_m$  is defined as,

$$\Delta T_m = \begin{cases} \min\{T_{wspec} - T_k, 0\}, & \text{for UNIDIRECT} \\ T_{wspec} - T_k, & \text{for BIDIRECT,} \end{cases} \quad (72)$$

The UNIDIRECT option shuts down cooling well, and the BIDIRECT option allows bidirectional heat transfer. In both cases, the BIDIRECT can simulate autoheater and autocooler. Their meanings are shown by Figure 68 [41].

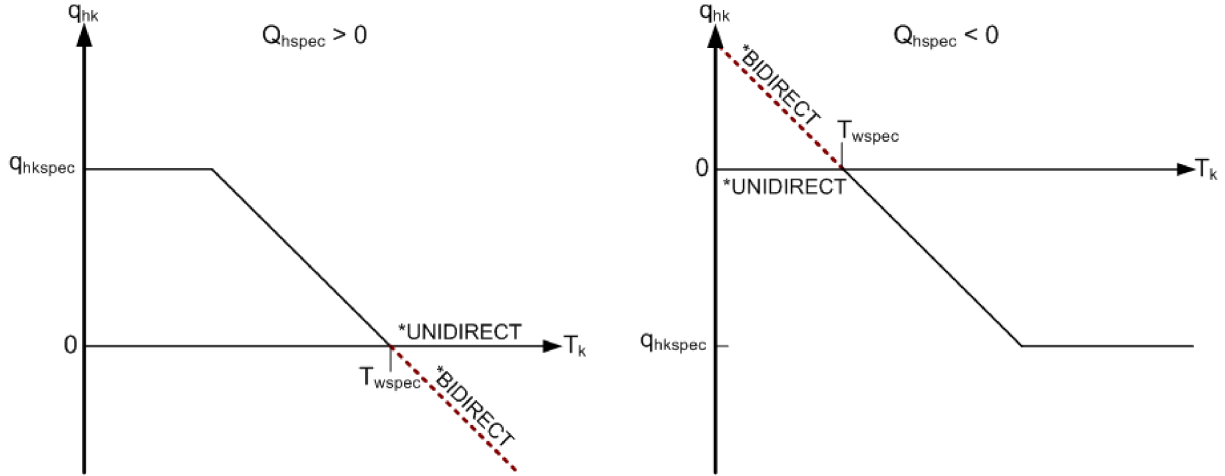


Figure 68: HTWELL: dual rate/temperature model [41]

**Example 9** The injection well operates at a fixed water rate 150 bbl/day. The injected water has a steam quality of 0.3 and temperature of 450 F. The production wells operate at fixed bottom hole pressure of 17 psi. The first production well uses temperature model at 600 F, and the second production well uses rate model with heat rate 3.4e6 Btu/day. The simulation period is 365 days. Figure 69, 70, 71, and 72 present bottom hole pressure of injection well, injection rate, total water production rate and total oil production rate. All results are compared with CMG STARS.

Figure 69 and 70 show the bottom hole pressure and injection rate, from which we can see the match is good except the first 20 days. CMG STARS shows convergence issue while our simulator is more robust. The total water and oil production rates have good match, which are demonstrated by Figure 71 and Figure 72, respectively.

#### 4.5.7 Heater Constraints

The heater controls can be applied simultaneously in one thermal model. They can be applied to different wells, and for a well, it may use a combination of constant heater, convective heater, and heater well model.

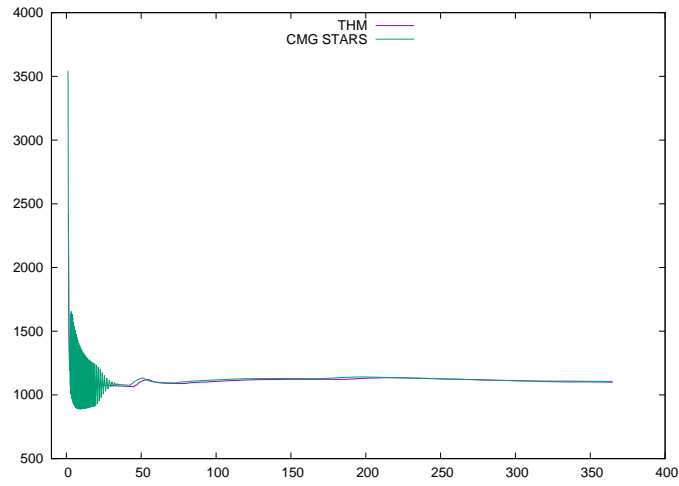


Figure 69: Example 9: injection well, bottom hole pressure (psi)

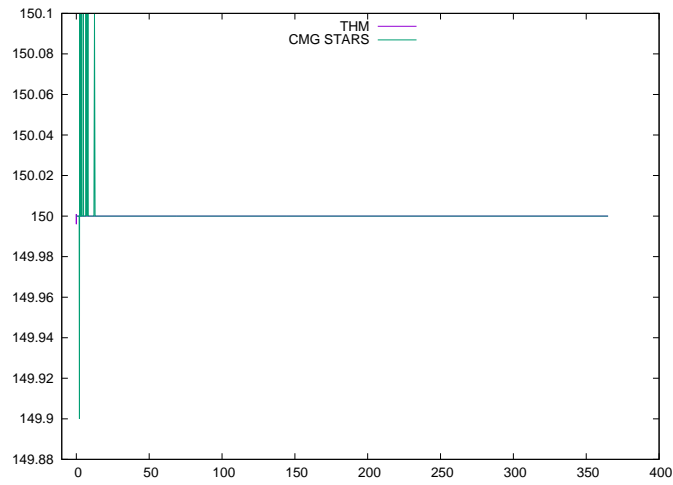


Figure 70: Example 9: water injection rate (bbl/day)

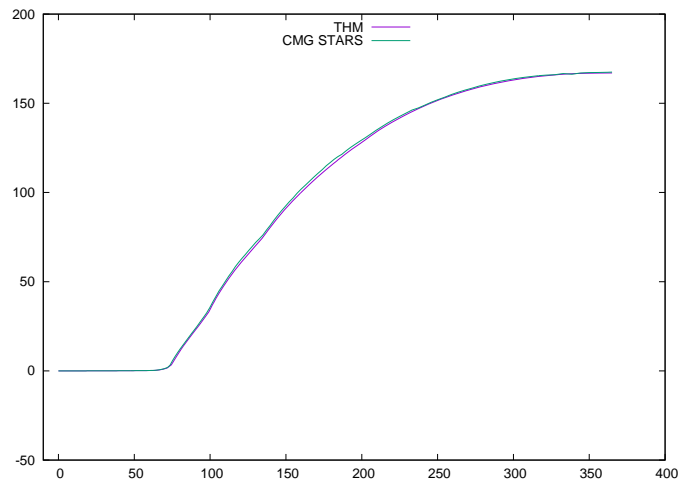


Figure 71: Example 9: water production rate (bbl/day)



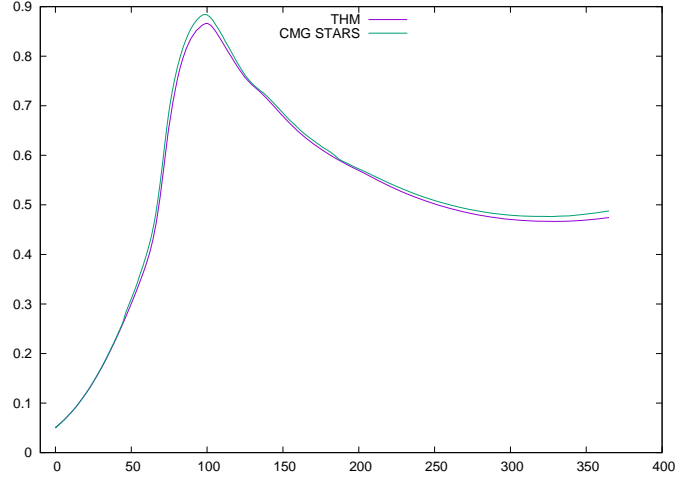


Figure 72: Example 9: oil production rate (bbl/day)

**Example 10** The injection well operates at maximal injection rate of 300 bbl/day water and maximal bottom hole pressure of 5,000 psi. Its steam quality is 0.5. The first production well operates at minimal bottom hole pressure of 17 psi and maximal liquid rate of 5 bbl/day. The temperature heater model is applied with a specify temperature of 600 F. The second production well operates at minimal bottom hole pressure of 17 psi and maximal oil rate of 4 bbl/day. The dual rate/temperature model is applied with a specify heat rate of  $3.4e6$  Btu/day and a specify temperature of 611. Constant heat transfer model is applied to each perforation at a constant heat rate of  $1e6$  Btu/day. The convective heat transfer model is also applied to each perforation at  $4e4$  Btu/day-F and a temperature setpoint of 500. Results are shown from Figure 73 to Figure 81. Bottom hole pressure, water rate and oil rate of each well are compared with CMG STARS.

All results match CMG STARS well. For injection well, Figure 73 shows CMG has convergence issues while our simulator and numerical methods are more stable.

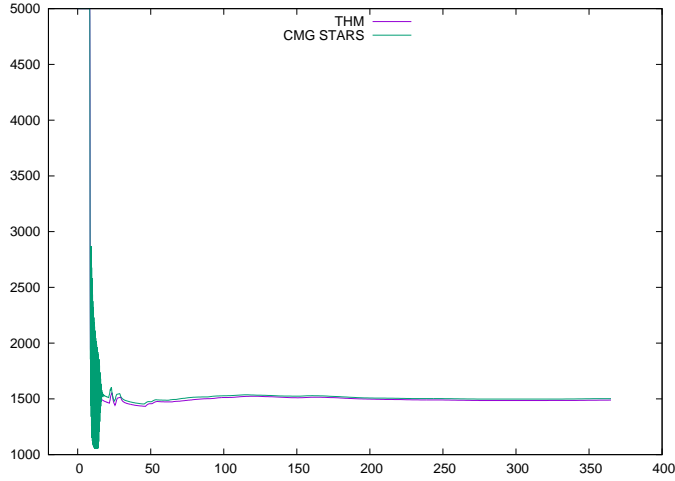


Figure 73: Example 10: injection well, bottom hole pressure (psi)

#### 4.5.8 Subcool Control

Subcool control is also known as steamtrap, which is used to prevent the production of live steam. It does this by keeping the well's flowing bottomhole pressure (and hence the pressure in the grid block containing the well) high enough that live steam does not appear in the well block [41].

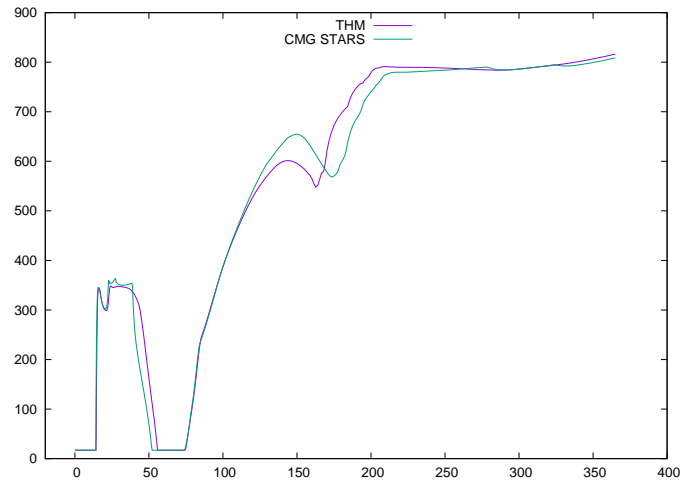


Figure 74: Example 10: first production well, bottom hole pressure (psi)

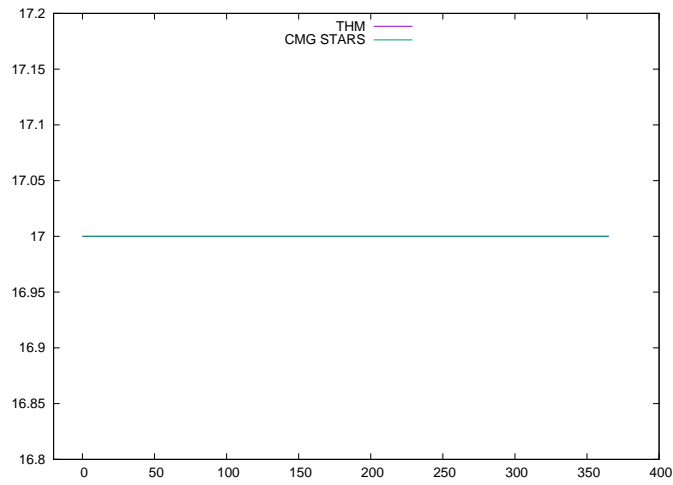


Figure 75: Example 10: second production well, bottom hole pressure (psi)

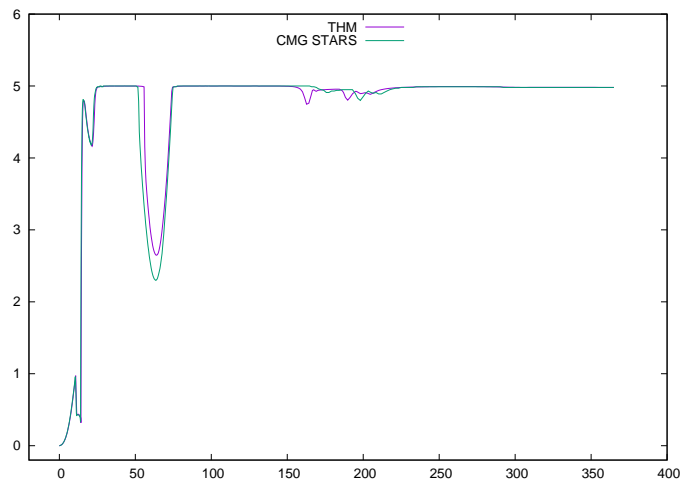


Figure 76: Example 10: water production rate (bbl/day), first production well

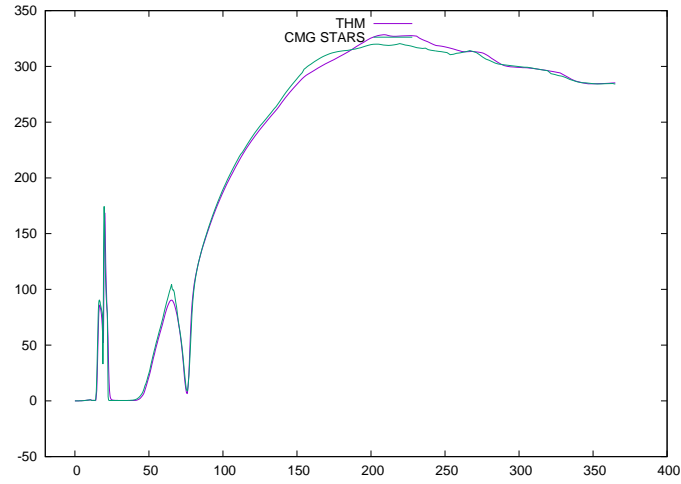


Figure 77: Example 10: water production rate (bbl/day), second production well

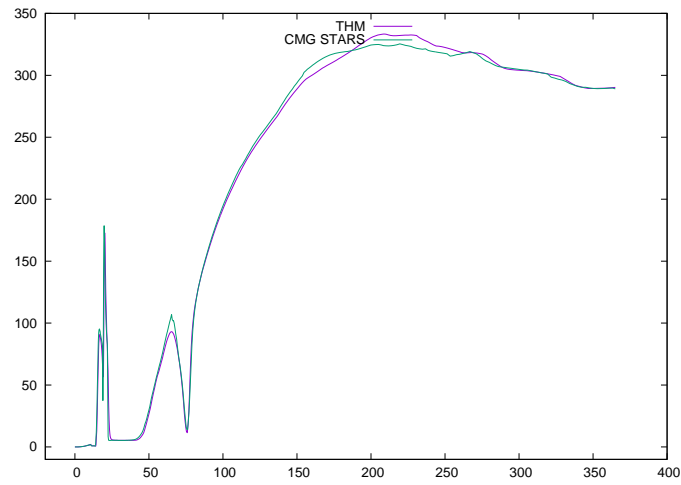


Figure 78: Example 10: total water production rate (bbl/day)

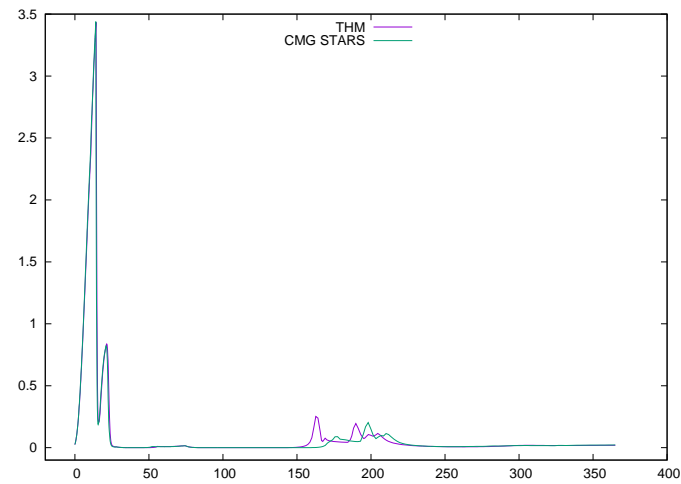


Figure 79: Example 10: oil production rate (bbl/day), first production well

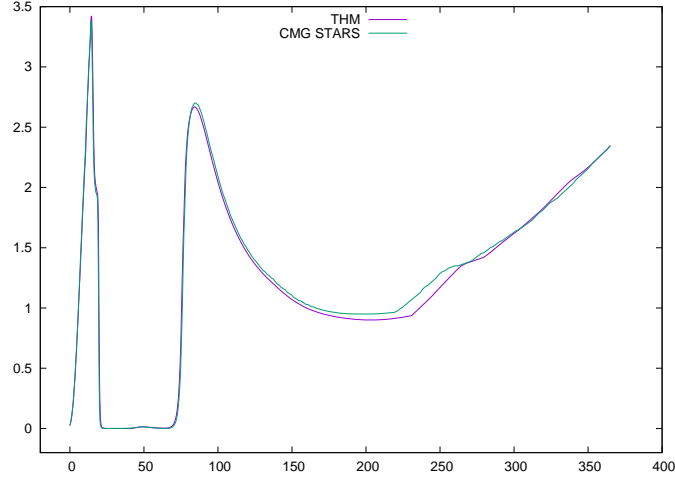


Figure 80: Example 10: oil production rate (bbl/day), second production well

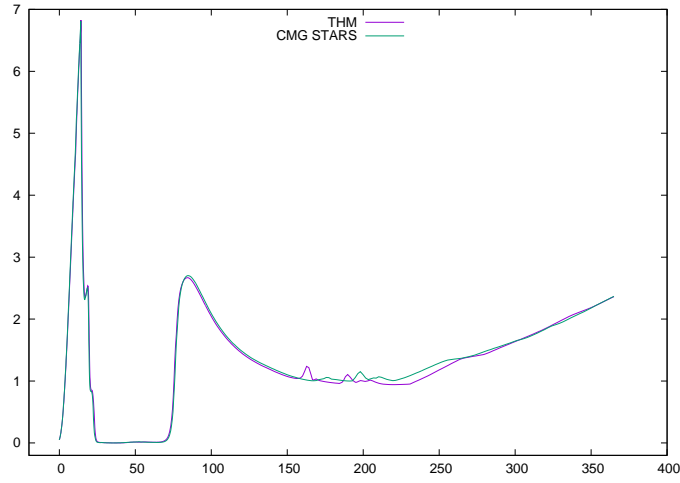


Figure 81: Example 10: total oil production rate (bbl/day)

The well constraint equation solved is written as,

$$T_{sat}(bhp) - T_k = c, \quad (73)$$

where  $c$  is a pre-defined temperature difference,  $T_{sat}$  is the steam saturation temperature corresponding to wellbore pressure at a perforation.

**Example 11** *The injection well operates at fixed injection rate of 100 bbl/day. Both production wells operate at fixed bottom hole pressure of 17 psi. The steamtrap temperature differences are 20 F and 30 F respectively. Bottom hole pressure of each well is presented, and total water and oil production rates are also presented, from Figure 82 to Figure 86.*

Figure 82 is bottom hole pressure of injection well, and our results match CMG STARS exactly. Figure 83 and Figure 84 show that the steamtrap works, as steam is injected into reservoir to heat reservoir and fluid, their temperature increases. The steamtrap works by increasing the wellbore pressure to prevent live steam production. The water and oil production also match CMG STARS well.

## 4.6 Scalability

The parallel computers from Compute Canada are employed. The Niagara supercomputer consists of 1500 nodes, and each node has 40 Intel Skylake cores at 2.4GHz, for a total of 60,000 cores. Each node has 202 GB (188 GiB) RAM, and EDR

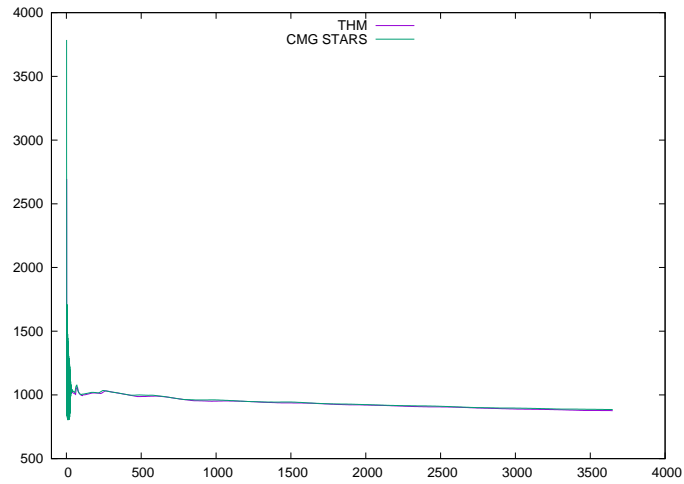


Figure 82: Example 11: injection well, bottom hole pressure (psi)

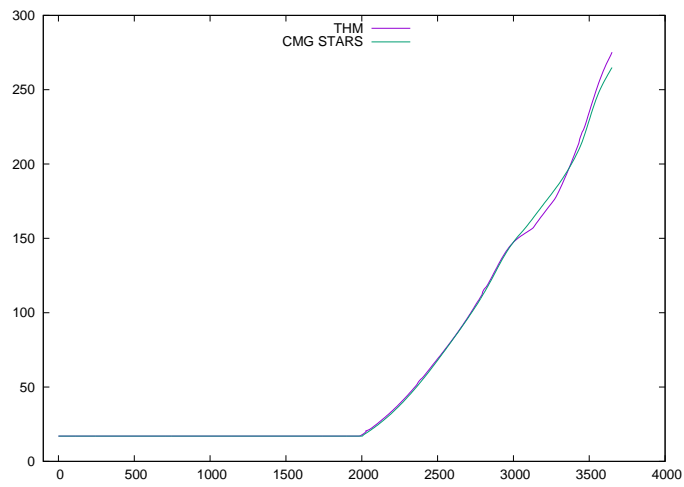


Figure 83: Example 11: first production well, bottom hole pressure (psi)

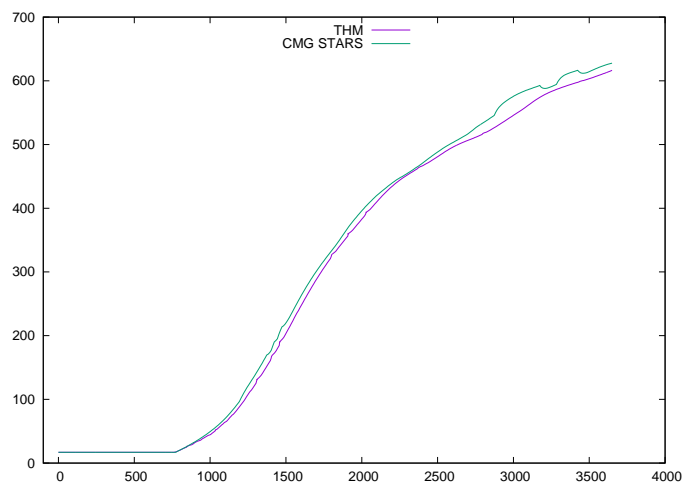


Figure 84: Example 11: second production well, bottom hole pressure (psi)

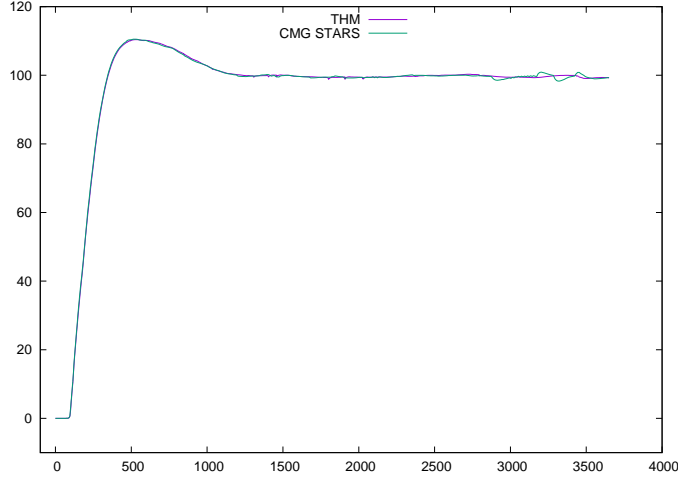


Figure 85: Example 11: water production rate (bbl/day)

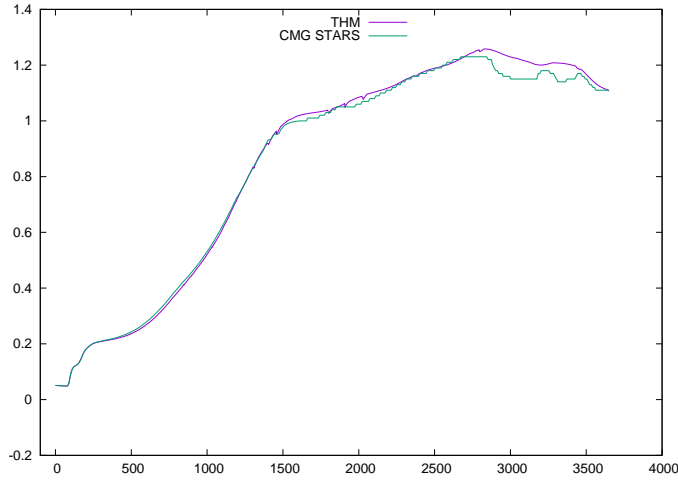


Figure 86: Example 11: oil production rate (bbl/day)

Infiniband network is used to communicate. The Cedar supercomputer has a hybrid architecture, which uses Intel E5-2683 v4 "Broadwell" at 2.1Ghz, E5-2650 v4 at 2.2GHz, Intel E7-4809 v4 "Broadwell" at 2.1Ghz, and Intel Platinum 8160F "Skylake" at 2.1Ghz. It has a total of 58,416 CPU cores for computation, and 584 GPU devices.

**Example 12** *This example studies a large thermal model with a grid dimension of  $360 \times 400 \times 1600$ , 230 million grid blocks. 12 nodes are employed using the Niagara supercomputer, and up to 192 CPU cores are used. The Newton method is applied with a tolerance of  $1e-6$  and maximal iterations of 10. The linear solver is BICGSTAB with a tolerance of  $1e-5$  and maximal iterations of 100. The preconditioner is the CPR-FPF method. Table 11 presents running time and memory used. Figure 87 shows the scalability.*

Table 11 shows that huge amount of memory is required, which is not possible for desktop computers. The running time and Figure 87 show the simulator, linear solver and preconditioner have good scalability. The solver and preconditioner can solve linear systems with billions of unknowns.

**Example 13** *This example studies a large thermal model with a grid dimension of  $360 \times 2000 \times 1600$ , 1.2 billion grid blocks. 120 nodes are employed using the Cedar supercomputer, and up to 960 CPU cores are used. The Newton method is applied with a tolerance of  $1e-10$  and maximal iterations of 10. The linear solver is BICGSTAB with a tolerance of  $1e-10$  and maximal iterations of 100. The preconditioner is the CPR-FPF method. Table 12 presents running time and memory used. Figure 88 shows the scalability.*

CPU cores	Total time (s)	Solver time (s)	Memory (GB)
24	2448.78	927.92	1945.92
48	1094.55	380.40	1959.28
96	545.20	194.81	1970.83
192	291.88	107.32	1994.25

Table 11: Summary of Example 12

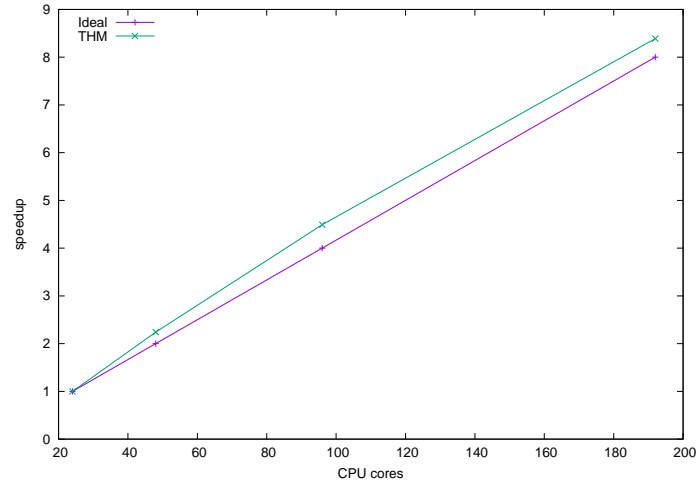


Figure 87: Example 12: scalability curve

Table 12 and Figure 88 show the simulator, linear solver and preconditioner have excellent scalability. The simulator can handle large-scale models, and the linear solver and preconditioner can solve linear systems with billions of unknowns.

CPU cores	Total time (s)	Solver time (s)	Memory (GB)
240	1802.24	934.92	9839
480	897.69	455.47	9906
960	474.29	227.89	9996

Table 12: Summary of Example 13

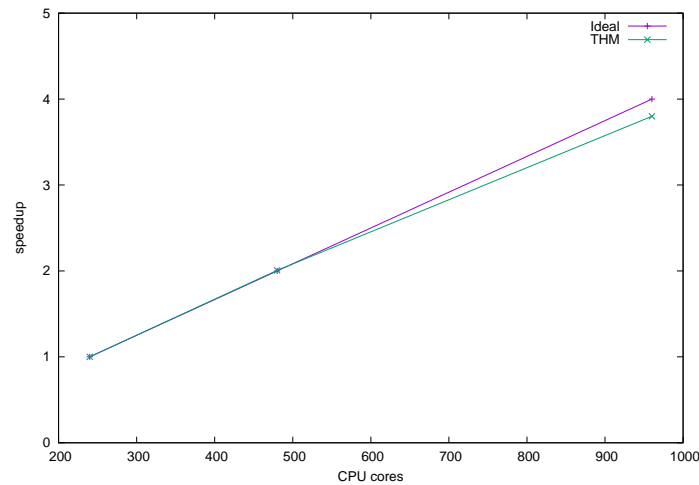


Figure 88: Example 13: scalability curve

## 5 Conclusions

This paper introduces a parallel thermal simulator. The numerical experiments show that our simulator can match commercial software and it has excellent scalability, which can handle extremely large-scale reservoir models.

## Acknowledgements

The support of Department of Chemical and Petroleum Engineering, University of Calgary and Reservoir Simulation Group is gratefully acknowledged. The research is partly supported by NSERC/AIEE/Foundation CMG and AITF Chairs.

## References

- [1] Ruijian He, Bo Yang, Hui Liu, Zhangxin Chen, A New In-Situ Combustion Simulator for Parallel Computers, arXiv: 1811.11992, 2018.
- [2] Peaceman, D. W. Interpretation of well-block pressures in numerical reservoir simulation. *Society of Petroleum Engineers Journal*, 18(03):183–194, 1978.
- [3] T. Al-Shaalan, H. Klie, A. Dogru, and M. Wheeler. Studies of robust two stage preconditioners for the solution of fully implicit multiphase flow problems. In *SPE Reservoir Simulation Symposium. 2009*.
- [4] Tareq Al-Shaalan, Larry S K Fung, and Ali H Dogru. A Scalable Massively Parallel Dual-Porosity Dual-Permeability Simulator for Fractured Reservoirs with Super-K Permeability. In *SPE Annual Technical Conference and Exhibition, 5-8 October, Denver, Colorado, 2003*.
- [5] J Barua and R N Horne. Improving the Performance of Parallel (and Serial) Reservoir Simulators. In *SPE Symposium on Reservoir Simulation, 6-8 February, Houston, Texas, 1989*.
- [6] H. Cao, T. Schlumberger, A. Hamdi, J. Wallis, and H. Yardumian. Parallel scalable unstructured cpr-type linear solver for reservoir simulation. In *SPE Annual Technical Conference and Exhibition. 2005*.
- [7] Mark C H Chien, Hamdi A Tchelepi, Hrant E Yardumian, and Wen H Chen. A Scalable Parallel Multi-Purpose Reservoir Simulator. In *SPE Reservoir Simulation Symposium, 8-11 June, Dallas, Texas, pages 17–30, 1997*.
- [8] K H Coats. In-Situ Combustion Model. *SPE Society of Petroleum Engineers of AIME*, 20:533–554, 1980.
- [9] K H Coats. Reservoir Simulation. In *Petroleum Engineering Handbook*, chapter 48, pages 20–48. 1987.
- [10] Dim Coumou, Stephan Matthäi, Sebastian Geiger, and Thomas Driesner. A parallel FE-FV scheme to solve fluid flow in complex geologic media. *Computers and Geosciences*, 34:1697–1707, 2008.
- [11] R B Crookston, W E Culham, and Wen H Chen. A Numerical Simulation Model for Thermal Recovery Processes. *Society of Petroleum Engineers Journal*, 19:37–58, 1979.
- [12] Ali H Dogru. Megacell Reservoir Simulation. *Journal of Petroleum Technology*, 52, 2000.
- [13] Ali H Dogru, K G Li, H.a. Sunaidi, W.a. Habiballah, Larry S K Fung, N Al-Zamil, D Shin, A E McDonald, and N K Srivastava. A Massively Parallel Reservoir Simulator for Large Scale Reservoir Simulation. In *SPE Reservoir Simulation Symposium, 14-17 February, Houston, Texas, 1999*.
- [14] Ali H Dogru, H A Sunaidi, Larry S K Fung, Walid A Habiballah, Nabil Al-Zamel, and K G Li. A Parallel Reservoir Simulator for Large-Scale Reservoir Simulation. *SPE Reservoir Evaluation & Engineering*, 5:11–23, 2002.
- [15] David a Edwards, Dayal Gunasekera, Jonathan Morris, Gareth Shaw, Kevin Shaw, Paul a Fjerstad, Jitendra Kikani, Jessica Franco, Viet Hoang, and Lisette Quettier. Reservoir Simulation : Keeping Pace with Oilfield Complexity. *Oilfield Review*, 23:4–15, 2012.
- [16] C. Feng, S. Shu, J. Xu, and C. Zhang. A multi-stage preconditioner for the black oil model and its openmp implementation. In *21st International Conference on Domain Decomposition Methods, 2012, France*.



- [17] Larry S K Fung and Ali H Dogru. Efficient multilevel method for local grid refinement for massively parallel reservoir simulation. In *ECMOR VII - 7th European Conference on the Mathematics of Oil Recovery*, 2000.
- [18] Janusz W Grabowski, Paul K Vinsome, Ran C Lin, Alda Behie, and Barry Rubin. A Fully Implicit General Purpose Finite-Difference Thermal Model For In Situ Combustion And Steam. In *SPE Annual Technical Conference and Exhibition, 23-26 September, Las Vegas, Nevada*, 1979.
- [19] X. Hu, W. Liu, G. Qin, J. Xu, and Z. Zhang. Development of a fast auxiliary subspace pre-conditioner for numerical reservoir simulators. In *SPE Reservoir Characterisation and Simulation Conference and Exhibition. 2011*.
- [20] John E Killough. Is Parallel Computing Ready for Reservoir Simulation ? A Critical Analysis of the State of the Art. In *SPE Annual Technical Conference and Exhibition, 3-6 October, Houston, Texas*, 1993.
- [21] H. Liu, K. Wang, and Z. Chen. A family of constrained pressure residual preconditioners for parallel reservoir simulations. *Numerical Linear Algebra with Applications*, 23:120–146, 2016.
- [22] Hui Liu, Kun Wang, and Zhangxin Chen. Large-scale reservoir simulations on ibm blue gene/q. In *Proceedings of The 3rd Intl. Conference on High Performance Computing and Applications, Shanghai, China, July 2015*.
- [23] Hui Liu, Kun Wang, Zhangxin Chen, Kirk E. Jordan, Jia Luo, and Hui Deng. A parallel framewrok for reservoir simulators on distributed-memory supercomputers. In *SPE-176045-MS, SPE/IATMI Asia Pacific Oil & Gas Conference and Exhibition, Nusa Dua, Indonesia, 20 22 October, 2015*.
- [24] J A Meijerink, D T Van Daalen, P J Hoogerbrugge, and R J A Zeestraten. Towards a More Effective Parallel Reservoir Simulator. In *SPE Symposium on Reservoir Simulation, 17-20 February, Anaheim, California*, 1991.
- [25] R T Mifflin, J W Watts, and A Weiser. A Fully Coupled, Fully Implicit Reservoir Simulator for Thermal and Other Complex Reservoir Processes. In *SPE Symposium on Reservoir Simulation, 17-20 February, Anaheim, California*, 1991.
- [26] Manish Parashar, John Wheeler, Gary Pope, Kefei Wang, and Peng Wang. A New Generation EOS Compositional Reservoir Simulator: Part II - Framework and Multiprocessing. In *SPE Reservoir Simulation Symposium, 8-11 June, Dallas, Texas*, 1997.
- [27] Barry Rubin and W Buchanan. A General Purpose Thermal Model. *Society of Petroleum Engineers Journal*, 25, 1985.
- [28] Sophie Verdiere, Lisette Quettier, Pierre Samier, and Alan Thompson. Applications of a parallel simulator to industrial test cases. In *SPE Reservoir Simulation Symposium, 14-17 February, Houston, Texas*, 1999.
- [29] J. Wallis, R. Kendall, and T. Little. Constrained residual acceleration of conjugate residual methods. In *SPE Reservoir Simulation Symposium, 1985*.
- [30] Baohua Wang, Shuhong Wu, Qiaoyun Li, Xiaobo Li, Hua Li, Chensong Zhang, and Jinchao Xu. A multilevel preconditioner and its shared memory implementation for new generation reservoir simulator. In *SPE-172988-MS, SPE Large Scale Computing and Big Data Challenges in Reservoir Simulation Conference and Exhibition, 15-17 September, Istanbul, Turkey, 2014*.
- [31] K. Wang, L. Zhang, and Z. Chen. Development of discontinuous galerkin methods and a parallel simulator for reservoir simulation. In *SPE-176168-MS, SPE/IATMI Asia Pacific Oil & Gas Conference and Exhibition, 20-22 October, 2015, Nusa Dua, Bali, Indonesia, 2015*.
- [32] Kun Wang, Hui Liu, and Zhangxin Chen. A scalable parallel black oil simulator on distributed memory parallel computers. *Journal of Computational Physics*, 301:19–34, 2015.
- [33] Kun Wang, Hui Liu, Jia Luo, and Zhangxin Chen. Parallel simulation of full-field polymer flooding. In *The 2nd IEEE International Conference on High Performance and Smart Computing (IEEE HPSC 2016)*.
- [34] Kun Wang, Hui Liu, Jia Luo, and Zhangxin Chen. A multi-continuum multi-phase parallel simulator for large-scale conventional and unconventional reservoirs. *Journal of Natural Gas Science and Engineering*, 33:483–496, 2016.

- [35] Peng Wang, S Balay, K Sepehrnoori, J Wheeler, J Abate, B Smith, and G A Pope. A Fully Implicit Parallel EOS Compositional Simulator for Large Scale Reservoir Simulation. In *SPE Reservoir Simulation Symposium, 14-17 February, Houston, Texas*, 1999.
- [36] Peng Wang, I Yotov, M Wheeler, T Arbogast, C Dawson, M Parashar, and K Sepehrnoori. A New Generation EOS Compositional Reservoir Simulator: Part I - Formulation and Discretization. In *SPE Reservoir Simulation Symposium, 8-11 June, Dallas, Texas*, 1997.
- [37] Yu-shu Wu, Keni Zhang, Chris Ding, Karsten Pruess, Erik Elmroth, and G S Bodvarsson. An efficient parallel-computing method for modeling nonisothermal multiphase flow and multicomponent transport in porous and fractured media. *Advances in Water Resources*, 25:243–261, 2002.
- [38] L. Zhang. A parallel algorithm for adaptive local refinement of tetrahedral meshes using bisection. *Numer. Math.*, 2:65–89, 2009.
- [39] L. Zhang, T. Cui, and H. Liu. A set of symmetric quadrature rules on triangles and tetrahedra. *J. Comput. Math*, pages 89–96, 2009.
- [40] Chen, Z. *Reservoir Simulation: Mathematical Techniques in Oil Recovery*. CBMS-NSF Regional Conference Series in Applied Mathematics. SIAM, 2007.
- [41] CMG. *STARS User’s Guide*. Computer Modelling Group Ltd., 2015.
- [42] Stone, H. L. Estimation of three-phase relative permeability and residual oil data. *Journal of Canadian Petroleum Technology*, 12(4), 1973.
- [43] Delshad, M. and Pope, G. A. Comparison of the three-phase oil relative permeability models. *Transport in Porous Media*, 4(1):59–83, 1989.
- [44] Stone, H. L. Probability model for estimating three-phase relative permeability. *Journal of Petroleum Technology*, 22(02):214–218, 1970.
- [45] Naar, J. and Wygal, R. J. Three-phase imbibition relative permeability. *Society of Petroleum Engineers Journal*, 1(04):254–258, 1961.
- [46] Corey, A. T., Rathjens, C. H., Henderson, J. H., and Wyllie, M. R. J. Three-phase relative permeability. *Journal of Petroleum Technology*, 8(11):63–65, 1956.
- [47] Coats, K. H. In-situ combustion model. *Society of Petroleum Engineers Journal*, 20(06):533–554, 1980.
- [48] Clapeyron, E. Memoir sur la puissance motrice de la chaleur. *Journal de l’cole Royale Polytechnique*, pages 153–190, 1834.
- [49] Redlich, O. and Kwong, J. N. On the thermodynamics of solutions. v. an equation of state. fugacities of gaseous solutions. *Chemical reviews*, 44(1):233–244, 1949.
- [50] Oklany, J. S. F. *An In-situ Combustion Simulator for Enhanced Oil Recovery*. PhD thesis, University of Salford, 1992.
- [51] Abou-Kassem, J. H. and Aziz, K. Handling of phase change in thermal simulators. *Journal of petroleum technology*, 37(09):1661–1663, 1985.
- [52] Crookston, R. B., Culham, W. E., and Chen, W. H. A numerical simulation model for thermal recovery processes. *Society of Petroleum Engineers Journal*, 19(01):37–58, 1979.
- [53] Coats, K. H. Simulation of steamflooding with distillation and solution gas. *Society of Petroleum Engineers Journal*, 16(05):235–247, 1976.
- [54] Hui Liu, Zhangxin Chen, Scalable linear solvers for sparse linear systems from large-scale numerical simulations, arXiv:1701.05913, 2016.
- [55] Hui Liu, Kun Wang, Bo Yang, Zhangxin Chen, Development of A Platform for Large-scale Reservoir Simulations on Parallel computers, arXiv:1602.05901, 2016.

- [56] Soave, G. Equilibrium constants from a modified redlich-kwong equation of state. *Chemical Engineering Science*, 27(6):1197–1203, 1972.
- [57] Peng, D. Y. and Robinson, D. B. A new two-constant equation of state. *Industrial & Engineering Chemistry Fundamentals*, 15(1):59–64, 1976.
- [58] Van der Waals, J. D. The equation of state for gases and liquids. *Nobel lectures in Physics*, 1:254–265, 1910.
- [59] Vinsome, Paul K and Westerveld, Joop D, A SIMPLE METHOD FOR PREDICTING CAP AND BASE ROCK HEAT LOSSES IN THERMAL RESERVOIR SIMULATORS, *Journal of Canadian Petroleum Technology*, 19(03), 87–90, 1980.
- [60] S. Lacroix, Y. V. Vassilevski, M. F. Wheeler, Decoupling preconditioners in the implicit parallel accurate reservoir simulator (IPARS), *Numerical Linear Algebra with Applications* 8 (8) (2001) 537–549.
- [61] R. Bank, T. Chan, The alternate-block-factorization procedure for systems of partial differential equations, *BIT Numerical ...* 4 (29) (1989) 938–954.
- [62] Sebastian Gries, On the Convergence of System-AMG in Reservoir Simulation, SPE-182630-PA, *SPE Journal*, 23(2), 589 - 597, 2018.
- [63] Z. Chen, *Reservoir Simulation Mathematical Techniques in oil recovery*, Society for Industrial and Applied Mathematics, Philadelphia, PA, 2007.